Environmental Research 212 (2022) 113340

Contents lists available at ScienceDirect

Environmental Research

journal homepage: www.elsevier.com/locate/envres

Review article

The application of transition metal-modified biochar in sulfate radical based advanced oxidation processes

Qingkai Shi [a,b,1], Si Deng [a,b,1], Yuling Zheng [a,b], Yinlin Du [a,b], Ling Li [a,b], Suzhao Yang [a,b], Gaoxia Zhang [a,b], Li Du [a,b], Guangfu Wang [a,b], Min Cheng [a,b,*], Yang Liu [c,**]

[a] College of Environmental Science and Engineering, Hunan University, Changsha, Hunan, 410082, China
[b] Key Laboratory of Environmental Biology and Pollution Control (Hunan University), Ministry of Education, Changsha, Hunan, 410082, China
[c] School of Minerals Processing and Bioengineering, Key Laboratory of Biohydrometallurgy of Ministry of Education, Central South University, Changsha, 410083, China

ARTICLE INFO

Keywords:
Biochar
Transition metal
Sulfate radical
Advanced oxidation processes
Organic pollutant degradation
Catalytic mechanism

ABSTRACT

Sulfate radical ($SO_4^{\bullet-}$) based advanced oxidation processes (SR-AOPs) is a very important chemical oxidation technology for the degradation of recalcitrant organic pollutants in water and has been well developed. Recently, transition metals or their oxides-modified biochar has been widely used as the catalyst to catalyze peroxymonosulfate (PMS) and peroxydisulfate (PS) in SR-AOPs due to their outstanding properties (e.g., large surface area, high stability, abound catalytic sites, and diversity of material design, etc.). These composite materials not only combine the respective beneficial characteristics of biochar and transition metals (or their oxides) but also often present synergistic effects between the components. In this review, we present the synthesis of different types of transition metal (or metal oxides)/biochar-based catalysts and their application in SR-AOPs. The catalytic mechanism, including the generation process of free radicals and other reaction pathways on the surface of the catalyst were also carefully discussed. Particular attention has been paid to the synergistic effects between the components that result in enhanced catalytic performance. At the end of this review, the future development prospects of this technology are proposed.

1. Introduction

With the continuous advancement of industrialization process, environmental problems become more and more serious. Among them, water pollution caused by various pollutants is one of the most central problems in the world (Ngoc Han et al., 2018). For example, the increased use of heavy metals (Arunakumara et al., 2013), antibiotics (Cheng et al., 2018b), pesticides (Hu et al., 2018), polycyclic aromatic hydrocarbons (PAHs) (Huang et al., 2017a), and polychlorinated biphenyls (PCBs) (Cheng et al., 2016) has caused serious damage to water sources (Petrie et al., 2015). Nowadays, numerous researchers have carried out series of studies on water pollution (Chen et al., 2019; Liu et al., 2020; Liu et al., 2022a, 2022b), and have developed various remediation methods, including physical (Cheng et al., 2018c), chemical (Liu et al., 2020), and biological (Liu et al., 2017) technologies.

Advanced oxidation process (AOPs) has been widely applied for the treatment of organic pollution (Cheng et al., 2017; Huang et al., 2020a). The commonly used AOPs, for example, sulfate radical ($SO_4^{\bullet-}$) based advanced oxidation processes (SR-AOPs) (Huang et al., 2021a, 2021b; Zhou et al., 2019), Fenton processes (Cheng et al., 2018a; Liu et al., 2019b) and photocatalysis, can produce reactive oxygen species (ROSs) with high redox potential (i.e., $SO_4^{\bullet-}$ and hydroxyl radicals (•OH)) for the effective degradation of organic contaminants (Cheng et al., 2016; Yang et al., 2019b). Among them, SR-AOPs have achieved great attention in the field of water treatment (Giannakis et al., 2021), because peroxymonosulfate (PMS) and peroxydisulfate (PS) are easy to be activated to generate free radicals to degrade contaminants in a broad operating pH range. Besides, the generated $SO_4^{\bullet-}$ has a high oxidation potential (E_0 = 2.5–3.1 V) and a long half-life (30–40 μs) (Xiao et al., 2020), which are beneficial to the degradation of contaminants. In SR-AOPs, transition metal catalysts including metals ions, such as Co^{2+} (Ling et al., 2010) , Fe^{2+} (Zou et al., 2013), Cu^{2+} (Zhang et al., 2013), and metals oxides such as Co_3O_4 (Deng et al., 2017), Fe_3O_4 (Tan et al., 2014) and CuO (Ji et al., 2011) have been widely used to activate PMS

* Corresponding author. College of Environmental Science and Engineering, Hunan University, Changsha, Hunan, 410082, China.
** Corresponding author.
E-mail addresses: chengmin@hnu.edu.cn (M. Cheng), liuyang_feiyang@163.com (Y. Liu).
[1] These authors contribute equally to this article.

https://doi.org/10.1016/j.envres.2022.113340
Received 23 April 2021; Received in revised form 4 March 2022; Accepted 17 April 2022
Available online 19 April 2022

and PS (Zhou et al., 2018). As shown in Eqs. (1)–(4), the activation mechanism of PMS and PS involves the reaction of valuable metals (M) with $HSO_5^-/S_2O_8^{2-}$.

$$M^{n+} + HSO_5^- \rightarrow M^{n+1} + SO_4^{\bullet-} + OH^- \quad (1)$$

$$M^{n+} + S_2O_8^{2-} \rightarrow M^{n+1} + SO_4^{\bullet-} + SO_4^{2-} \quad (2)$$

$$M^{n+1} + HSO_5^- \rightarrow M^{n+} + SO_5^{\bullet-} + H^+ \quad (3)$$

$$M^{n+1} + S_2O_8^{2-} \rightarrow M^{n+} + S_2O_8^{\bullet-} \quad (4)$$

However, the application of transition metal catalysts is usually limited by agglomeration and poor stability of catalysts, and large dissolution of metal ions (Wang et al., 2019b). The formation of composite catalysts by loading transition metal catalysts on the carriers is a feasible way to overcome these drawbacks (Li et al., 2017). In recent research, biochar (BC) derived from pyrolyzing biomass under oxygen-deficient atmosphere has been widely used as support for transition metal catalysts to synthesize composite catalysts with high activity in SR-AOPs (Faheem et al., 2020; Lee and Park, 2020; Li et al., 2020c; Lopes and Astruc, 2021; Premarathna et al., 2019). Biochar with high specific area can not only ensure the uniform distribution of transition metal-based materials and thus greatly reduces their agglomeration, but also can provide electrons and accelerate the transfer of electrons in the catalytic reactions (Zhang et al., 2020). Besides, the transform of metal ions with different valence will be increased, which can indirectly increase the production rate of free radicals (Pan et al., 2021). What's more, the conversion of metal ions with different valence states exists widely in catalytic systems, such as Fe^{2+}/Fe^{3+} and Co^{2+}/Co^{3+}, which can make these catalysts high catalytic capabilities (Yuan et al., 2017). It should be noted that in these transition metal-loaded biochar materials based SR-AOPs, both free radical and non-free radical ways are involved in the degradation of pollutants. In the free radical pathway, PMS/PS reacts with transition metals attached to the surface of biochar to produce $SO_4^{\bullet-}$ (Ushani et al., 2020), and other free radicals (i.e., •OH and $O_2^{\bullet-}$) are also generated in the reaction system (Xiao et al., 2018). While in the non-free radical pathway, functional groups on the surface of biochar can directly transfer electrons from contaminants to PMS/PS (Ruan et al., 2019). Under many situations, the free radical pathway plays a vital role while the non-free radical pathway plays a secondary role in such system. What is interesting is that multifunctional micromotors based on carbon nanomaterials can propel automatically in the wastewater and provide efficient dynamic oxidation platforms for AOPs, improving the efficiency of water treatment, which is another aspect of transition metal-modified biochar materials in wastewater treatment (Lee et al., 2018; Maria-Hormigos et al., 2018).

In this review, the research development and progress of transition metal/biochar-based catalysts in SR-AOPs are reviewed, aiming to discuss their efficient application for the removal of pollutants from wastewater. The applications of different transition metal-loaded biochar composites in the PMS/PS catalytic system are summarized and discussed. The mechanism of different active sites on biochar and transition metal was particularly revealed. This review also points out the different reaction pathways (free radical pathway and non-free radical pathway) in such reaction systems. Finally, the directions of future research are proposed, which will contribute to wastewater treatment and environmental remediation.

2. Fe species modified BC for persulfate catalysis

2.1. Fe oxide/BC

Iron-based catalysts have received much attention because of their excellent catalytic performance, non-toxicity and environmental friendliness (Sun et al., 2019; Wang et al., 2019a; Xiao et al., 2020). In 2017, pine and nFe_3O_4 were used to produce nFe_3O_4/biochar composite for PS activation (Ouyang et al., 2017). The pretreated pine needles were pyrolyzed in muffle furnace to produce biochar samples, and then the samples reacted with iron species in solution to produce nFe_3O_4/-biochar. Experiments showed that 1, 4-dioxane degradation efficiency by nFe_3O_4/biochar/PS after 120 min reaction reached 98.0%, which is significantly higher than those of nFe_3O_4/PS and biochar/PS. As shown in Fig. 1a, in the nFe_3O_4/biochar/PS system free radical was generated through three main processes: 1) the reactive sites of nFe_3O_4 transferred an electron from Fe^{2+} to PS to generate $SO_4^{\bullet-}$, 2) –COOH and C–OH could activate PS, 3) •OH was produced through $SO_4^{\bullet-}$ reacting with H_2O. In 2019, Rong et al. (2019) used banana peels as raw and processed material to synthesize magnetic biochar (γ-Fe_2O_3@BC) by a facile one-pot thermal process to activate PS for degradation of various organic contaminants. The catalyst had abundant active sites ascribed to large surface, well-dispersed iron specie, numerous oxygen functional groups and rich doped nitrogen. Bisphenol A (BPA) got an entire removal with an observed rate constant of 0.1849 min^{-1} within 20 min (0.0956 min^{-1} of BC). What's more, about 74.1% of BPA can be removed after 4 cyclical runs, indicating that the magnetic biochar has relatively high reusability and stability. The reduction of catalytic performance was likely attributed to the surface chemical structure changes, the consumption of active sites and the coverage of intermediates on catalyst surface active sites. Although the removal efficiency of pollutants was reduced, the X-ray diffraction (XRD) pattern of γ-Fe_2O_3@BC did not change significantly, and the concentrations of iron ion leaching during the four cycles were 0.087, 0.081, 0.14 and 0.096 mg/L respectively, which only accounted for about 0.2% of the iron amount of catalyst. To determine the reaction mechanism, radical quenching experiments were carried out. Because ethanol was an efficient scavenger of both $SO_4^{\bullet-}$ and •OH, while t-butanol was only an efficient quencher of •OH, they were used as radical scavengers. When the ratio of scavenger to PS increased to 1000:1, the degradation efficiency of BPA decreased significantly after 60 min (degradation efficiency was reduced from 100% to 38.92% (ethanol) and 15.48% (t-butanol)), indicating that $SO_4^{\bullet-}$ and •OH were involved in the degradation of BPA, and •OH was the dominant radical for BPA degradation. In addition, it was also proves this conclusion that rate constants decreased 0.1849 min^{-1} to 0.0092 min^{-1} for ethanol and 0.0030 min^{-1} for t-butanol respectively (n([scavenger/PS] = 1000)). In previous reports, some researchers also found that •OH was the dominant radical for BPA degradation in SR-AOPs. They thought the possible reason was the rate constant of •OH was greater than that of $SO_4^{\bullet-}$ (Arnold et al., 2017; Ren et al., 2021; Sanchez-Polo et al., 2013). The mechanism of the oxidation process (Fig. 1b) was proposed by the authors. The O–O bond of PS could be weakened by the active sites of biochar, and •OH was produced via oxidizing the absorbed H_2O or OH^- (Eq. (5) and Eq. (6)) (Duan et al., 2015, 2018). On the other hand, the persistent free radicals (PFRs) in biochar transferred electron to oxygen molecule to generate $O_2^{\bullet-}$ (Eq. (7) and Eq. (8)), which further reacted with $S_2O_8^{2-}$ to produce $SO_4^{\bullet-}$ (Khachatryan et al., 2011). It was suggested that biochar was not only a supporter to load γ-Fe_2O_3 nanoparticles, but also an excellent electron transfer support during the process.

$$SO_4^{\bullet-} + H_2O \rightarrow HSO_4^- + \bullet OH \quad (5)$$

$$SO_4^{\bullet-} + OH^- \rightarrow SO_4^{2-} + \bullet OH \quad (6)$$

$$BC_{surface}\text{ - }OOH + S_2O_8^{2-} \rightarrow SO_4^{\bullet-} + BC_{surface}\text{ - }OO\bullet + HSO_4^- \quad (7)$$

$$BC_{surface}\text{ - }OH + S_2O_8^{2-} \rightarrow SO_4^{\bullet-} + BC_{surface}\text{ - }O\bullet + HSO_4^- \quad (8)$$

Another study prepared Fe, N co-doped biochar (Fe-N-BC) by pyrolyzing wheat straw, urea and iron salts for activating PS to remove organic contaminants (Li et al., 2020b). The doping of iron oxide not only made biochar magnetic and easy to separate, but also affected its ability for PS activation. Almost all acid orange (AO7) was removed

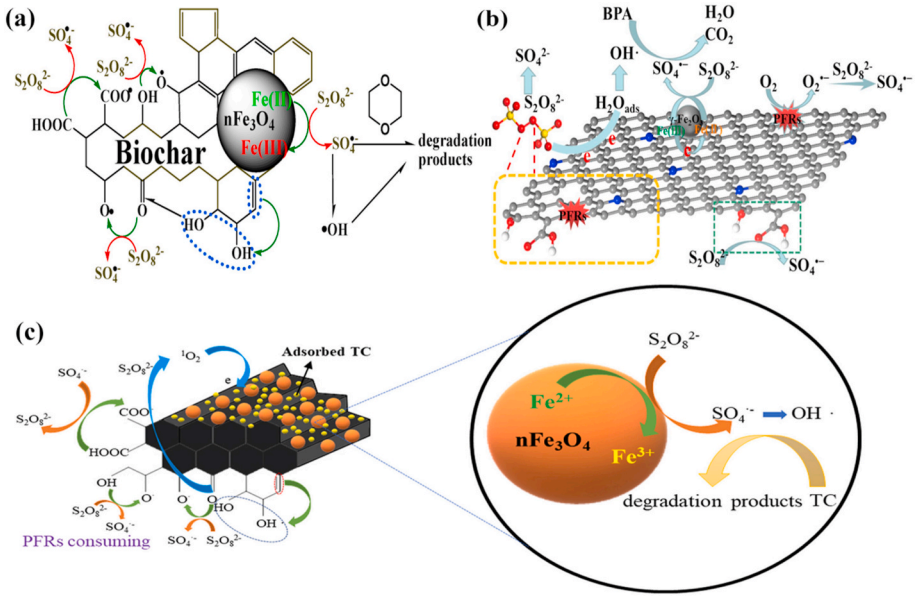

Fig. 1. (a) Proposed mechanism of nFe_3O_4/biochar activating persulfate for 1, 4-dioxane degradation. Adapted with permission from Ref. (Ouyang et al., 2017), Copyright 2017 Elsevier. (b) Possible mechanism of persulfate activation by γ-Fe_2O_3@BC for BPA degradation. Adapted with permission from Ref. (Rong et al., 2019), Copyright 2019 Elsevier. (c) Proposed mechanism of PS activation by OBC-Fe_3O_4 for TC degradation. Adapted with permission from Ref. (Pi et al., 2019), Copyright 2019 Elsevier.

within 90 min in Fe-N-BC/PS system, while only 7.8%, 23.3%, and 41.1% was removed in PS system, Fe-BC system, and Fe-N-BC system, respectively. The mechanism of AO7 degradation involves free radical and non-free radical pathway. To identify the different ROSs during the reaction process, the quenching experiments and electron paramagnetic resonance (EPR) were carried out. Ethanol, t-butanol, furfuryl alcohol, p-benzoquinone, and KI were employed as a quencher of $SO_4^{\bullet-}$/•OH, •OH, $^1O_2$, $O_2^{\bullet-}$, and surface-bounded radical, respectively. When each quencher was used singly, the AO7 removal was inhibited markedly, with a decrease of rate constant, revealing that $SO_4^{\bullet-}$, •OH, $O_2^{\bullet-}$, and $^1O_2$ were generated in the Fe-N-BC/PS system. DMPO (5,5-Dimethyl-1-pyrroline N-oxide) and TEMP (2,2,6,6-tetramethyl-4-piperidinol) were adopted as the spin trapping agents to detect $SO_4^{\bullet-}$, •OH, $O_2^{\bullet-}$, and $^1O_2$, respectively. The typical EPR signals of DMPO-OH, DMPO-SO_4 and DMPO-O_2^- could be observed, and a representative triple EPR spectrum (1:1:1) corresponding to the oxidized TEMP by $^1O_2$ appeared, which consisted with the free radical quenching results. In the Fe-N-BC/PS system, Fe species activates PS to generate $SO_4^{\bullet-}$, and then •OH was produced by $SO_4^{\bullet-}$ reacting with H_2O or OH^-. The PFRs produced during biochar pyrolysis could not only activate PS directly, but also transfer electrons to oxygen molecules to generate $O_2^{\bullet-}$. The widespread use of antibiotics has made tetracycline (TC) an important pollutant, thus Pi et al. (2019) had done relevant research on catalyzing PS to remove TC with biochar supported magnetite particles (OBC–Fe_3O_4) as a catalyst. The results show 92.3% of TC was removed within 2 h with PS dosage of 10 mM, OBC-Fe_3O_4 dosage of 0.4 g/L and pH of 3.0. The high removal efficiency could be ascribed to Fe_3O_4 particles and abundant oxygen-containing groups on the surface. As shown in Fig. 1c, author proposed mechanism also contained free radical and non-free radical pathway. Fe^{2+} reacted with PS to form $SO_4^{\bullet-}$, and then $SO_4^{\bullet-}$ reacted with H_2O/OH^- to form •OH. In addition, $O_2^{\bullet-}$ and $^1O_2$ were also involved in the degradation of TC, and $^1O_2$ could be generated through Eq. (9) and Eq. (10). Moreover, it was found that excessive PS leaded self-quenching of $SO_4^{\bullet-}$ (Eq. (11) and Eq. (12)). In addition to PS, PMS also could be activated to produce $SO_4^{\bullet-}$ for pollutants treatment. For example, Fu et al. (2019b) synthesized graphitized porous biochar supported Fe_3O_4 for activating PMS to degrade p-hydroxybenzoic acid (HBA). With K_2FeO_4 as the modifier and black powders obtained from Myriophyllum aquaticum as the precursor, the Fe_3O_4/MC composites were prepared at different pyrolysis temperatures (600, 700 and 800 °C). Due to the mesopores ratio and high graphitization degree, Fe_3O_4/MC700 and Fe_3O_4/MC800 showed better degradation efficiency than Fe_3O_4/MC600. The author proposed a similar two-pathway mechanism of this process, and revealed that $SO_4^{\bullet-}$ was also the dominant free radical and non-free radical pathway performed as electro-transfer was the recessive way during the degradation process. Interestingly, the author proposed that Fe^{3+} was reduced by $O_2^{\bullet-}$ rather than $SO_4^{\bullet-}$, due to the fact that the reduction potential of $O_2^{\bullet-}/O_2$ was −0.33 V, which was more negative than that of Fe^{3+}/Fe^{2+} (0.77 V), making it thermodynamic possible (Eqs. (13)–(15)). Similarly, the author pointed out that high levels of PMS concentration would lead to the self-quenching of $SO_4^{\bullet-}$ and •OH via Eq. (11), Eqs. (16)–(17). Besides, $SO_4^{\bullet-}$ and •OH would be transformed to $SO_5^{\bullet-}$ with lower oxidation ability, according to Eq. (18) and Eq. (19).

$$O_2^{\bullet-} + O_2^{\bullet-} + 2H^+ \rightarrow {}^1O_2 + 2H_2O_2 \quad (9)$$

$$O_2^{\bullet-} + \bullet OH \rightarrow {}^1O_2 + OH^- \quad (10)$$

$$SO_4^{\bullet-} + SO_4^{\bullet-} \rightarrow S_2O_8^{2-} \quad (11)$$

$$S_2O_8^{2-} + SO_4^{\bullet-} \rightarrow S_2O_8^{\bullet-} + SO_4^{2-} \quad (12)$$

$$HSO_5^- \rightarrow H^+ + SO_5^{2-} \quad (13)$$

$$SO_5^{2-} + H_2O \rightarrow O_2^{\bullet-} + SO_4^{2-} + H^+ \quad (14)$$

$$Fe^{3+} + O_2^{\bullet-} \rightarrow Fe^{2+} + O_2 \quad (15)$$

$$SO_4^{\bullet-} + \bullet OH \rightarrow HSO_5^- \quad (16)$$

$$\bullet OH + \bullet OH \rightarrow H_2O_2 \quad (17)$$

$$SO_4^{\bullet-} + HSO_5^- \rightarrow SO_4^{2-} + H^+ + SO_5^{\bullet-} \quad (18)$$

$$\bullet OH + HSO_5^- \rightarrow H_2O + SO_5^{\bullet-} \quad (19)$$

Sludge is an important raw material for the preparation of biochar. In 2018, Yu et al. (2019) produced magnetic nitrogen-doped sludge biochar (MS-biochar) by one-pot synthetic method, the obtained MS-biochar was used to catalyze PS for the degradation of TC. Further studies proved that graphitic carbon, iron oxides and nitrogen species were the namely catalytic sites for PS. And the author identified that the system was absolutely controlled by free radical pathway rather than the non-free radical active substance by quenching and electron spin resonance spectroscopy. The generation of free radicals may be explained by the following two reasons. Firstly, when the H_2O and $S_2O_8^{2-}$ were both absorbed on the surface of carbon matrix, the weakened and activated

$S_2O_8^{2-}$ would oxidize H_2O molecule to form •OH radicals (Deng et al., 2018). Secondly, $S_2O_8^{2-}$ was activated to generate $SO_4^{\bullet-}$, and then $SO_4^{\bullet-}$ reacted with H_2O to produce •OH radicals (Eqs. (20)–(23)). Similarly, Chen et al. (2019) found that anaerobic digested sludge derived biochar supported iron oxides (Fe-ADSBC) could improve the degradation efficiency of sulfamethazine (SMT). They found that the synthesis temperature of biochar possessed a great influence on the catalytic performance of the material. Less than 4.6% of SMT could be degraded by PS without activation while Fe-ADSBC 600 and Fe-ADSBC 800 attained 33.3% and 61.8% removals in 90 min, whereas Fe-ADSBC 1000 yielded a complete SMT oxidation within 60 min due to the iron species transformed from Fe_3O_4 to FeO with increased temperatures. Therefore, it could be found that graphitic biochar supported FeO was more active than Fe_3O_4 nanocrystals during PS activation.

$$S_2O_8^{2-} + H_2O \rightarrow \bullet OH + 2SO_4^{2-} + H^+ \quad (20)$$

$$S_2O_8^{2-} + \equiv Fe(II) \rightarrow \equiv Fe(III) + SO_4^{\bullet-} + SO_4^{2-} \quad (21)$$

$$S_2O_8^{2-} + CM\equiv sites \rightarrow CM\equiv sites^* + SO_{4ads or}^{\bullet-} + SO_4^{2-} \quad (22)$$

$$SO_{4ads or}^{\bullet-} + H_2O \rightarrow \bullet OH + SO_4^{2-} + H^+ \quad (23)$$

A series of studies on bamboo biochar (BB) have been conducted by Dong's research team since 2017 (Dong et al., 2017, 2018a, 2018b, 2019). In 2017, they synthesized this low-cost composite catalyst (Fe_3O_4-BB) for the degradation of PAHs in the remediation of sediments (Dong et al., 2017). Fe_3O_4 particles with a spherical shape were coated on the porous BB surface successfully. At a catalyst concentration of 3.33 g/L, a PS concentration of 1.7×10^{-5} M and pH of 3.0, Fe_3O_4-BB/PS significantly improved the degradation efficiency to 86%, as compared with PS of 14% and Fe_3O_4-BB of 21%. Study revealed that Fe(III)/Fe(II)'s conversion and high electron transfer rate in BB remarkably improved the generation of $SO_4^{\bullet-}$ that demonstrated the synergistic effect between $S_2O_8^{2-}$ and Fe_3O_4. They also used BB combined with iron oxide to catalyze PS to remove 4-nonylphenol from river sediments in 2019 (Dong et al., 2019). At a catalyst concentration of 3.33 g/L, PS concentration of 2.3×10^{-5} M and pH of 3.0, the degradation efficiency of 4-nonylpheno achieved 85%, which was better than that of PS (20%) and Fe_3O_4-BB (10%). Very interestingly, they did HepG2 cell viability assay and found that this catalyst had low potent cytotoxic effect, which is likely ascribed to the reductive capacity of biochar surface (Dong et al., 2018b).

2.2. nZVI/BC

In recent years, nanomaterials had attracted widespread attention, because of their small size and excellent surface effect. Nano zero valent iron (nZVI) not only had the properties of ZVI, but also had larger specific surface area, higher reaction activity and better adsorption performance. However, there were still some problems in practical applications, for example, nZVI was easily oxidized by air, and the oxide film would reduce the reaction rate and affect the material activity. Moreover, nZVI had high reducibility, which will harm the environment. NZVI, as an alternative source of iron ion, has been successfully combined with BC as PS activator (Hussain et al., 2017; Pang et al., 2019). In 2019, based on the degradation of imidacloprid through PS oxidation, series studies were taken to compare the different performances among magnetic biochar, nanoscale nFe_3O_4 and nZVI (Hayat et al., 2019). The most efficient degradation was achieved by nZVI/SPS (sodium PS) system, which suggested that nZVI/PS system was an efficient wastewater treatment technology.

NZVI/biochar composites generally performed excellently in terms of PS/PMS activation. Such as, in a pioneering work, Yan et al. (2015) synthesized nZVI/biochar composites to remove the trichloroethylene (TCE). The biochar was synthesized by pyrolysis of rice hull and supported nZVI through stirring. The 99.4% TCE was degraded within 5 min in the presence of nZVI/BC (4.5 mM, nZVI to BC mass ratio was 1:5) and PS (4.5 mM). However, the presence of iron ions in the solution indicated that some of nZVI was turned into dissolved iron. The formed Fe^{2+} can react with PS and lead to the production of $SO_4^{\bullet-}$. Besides, solid $FeSO_4$ was generated as Eqs. (24)–(29) and promoted the formation of $SO_4^{\bullet-}$. As illustrated in Fig. 2a, under acidic and neutral pH, $SO_4^{\bullet-}$ was the dominant radical, but when the pH was 8.0, $SO_4^{\bullet-}$ can react with OH^- to produce •OH, finally, •OH became the main radical when pH reached 10.0 in the solution. In this system, the activation of PS was ascribed to two reasons: 1) the redox action of Fe^{2+}/Fe^{3+}, 2) the electron-transfer mediator of the biochar oxygen functional groups contributed to the degradation of TCE. Similarly, in 2019, Jiang et al. (2019) prepared a Fe^0 functionalized biochar composite (Fe-BC-700) to activate PMS for removing BPA. It was found that BPA (20 mg/L) could be completely removed under optimal conditions (0.2 g/L PMS and 0.15 g/L catalyst) in 5 min by Fe-BC-700. The author revealed that both the free radical mechanism and the non-free radical mechanism as shown in Fig. 2b were involved in this system. In the activated free radical mechanism, Fe^0 was the supply source of iron ions. Fe^0 reacted with PMS to generate $SO_4^{\bullet-}$ and Fe^{2+}, furthermore Fe^{2+} could also react with PMS to generate $SO_4^{\bullet-}$, while the generated Fe^{3+} reacted with PMS to produce Fe^{2+} (Eqs. (30)–(32)) (Oh et al., 2016; Takdastan et al., 2018). For the non-free radical mechanism, the surface of this composite with abundant functional groups could accelerate the electron transfer to enhance the degradation efficiency of BPA. In a recent work, ZVI-Sludge Derived Biochar (SDBC) was synthesized through the one-step of pyrolysis (Wang et al., 2020). SDBC was made by pyrolyzed dried sludge at 400 °C for 2 h, and ZVI-SDBC was prepared by fulling mixing the dried sludge with the $NaBH_4$ solution and then pyrolyzed at 400 °C for another 2 h. The results show 99.0% of AO7 was dislodged in the PS/ZVI-SDBC system, while only 10.3% and 16.6% of AO7 was removed by PS or ZVI-SDBC, respectively. It was also suggested both free radical and non-free radical pathways contributed to the degradation, and the contribution ratio of •OH, $SO_4^{\bullet-}$, $^1O_2$ and other ROSs were 71.9%, 9.0%, 10.6%, and 8.4%, respectively in pH of 7.0, while those were 86.1%, 7.9% 4.9% and 1.1% in the case of pH 9.0, respectively, indicating •OH was the dominant reactive radical.

$$Fe^0 + SO_4^{2-} + 2H_2O \rightarrow FeSO_4(s) + 2OH^- + H_2 \quad (24)$$

$$Fe^{2+} + H_2O \rightarrow Fe^{3+} + OH^- + 1/2H_2 \quad (25)$$

$$Fe^{3+} + 3OH^- \rightarrow Fe(OH)_3 \quad (26)$$

$$Fe^{3+} + 3H_2O \rightarrow Fe(OH)_3 + 3H^+ \quad (27)$$

$$Fe(OH)_3 \rightarrow FeOOH + H_2O \quad (28)$$

$$FeOOH + SO_4^{2-} + H_2O \rightarrow FeSO_4(s) + 2OH^- + H_2 + O_2 \quad (29)$$

$$Fe^0 + 2HSO_5^- \rightarrow Fe^{2+} + 2SO_4^{\bullet-} + 2OH^- \quad (30)$$

$$Fe^{2+} + HSO_5^- \rightarrow Fe^{3+} + SO_4^{\bullet-} + OH^- \quad (31)$$

$$Fe^{3+} + HSO_5^- \rightarrow Fe^{2+} + SO_5^{\bullet-} + H^+ \quad (32)$$

Recently, granular red mud reinforced by zero-valent iron (Fe@GRM) was prepared by heating red mud, maize straw and bentonite (Du et al., 2020). The pretreated red mud, maize straw and bentonite were stirred according to a mass ratio of 2:1:0.5. And then it was sintered for 1 h under anoxic conditions at 900 °C. Maize straw as the reducing agent reduced iron oxidize to ZVI that loaded in the composite. The removal efficiency of AO7 achieved 90.78% using Fe@GRM/PS, while only 18.15% when Fe@GRM/PS was used. In Fe@GRM/PS system, AO7 was adsorbed onto the surface of Fe@GRM, and degraded by the $SO_4^{\bullet-}$ produced from the reaction of PS and Fe^0, and a small portion of them was directly oxidized by Fe^0. Some other studies also found that for aromatic pollutants which are easy to be adsorbed, the degradation can be enhanced through a surface action mechanism.

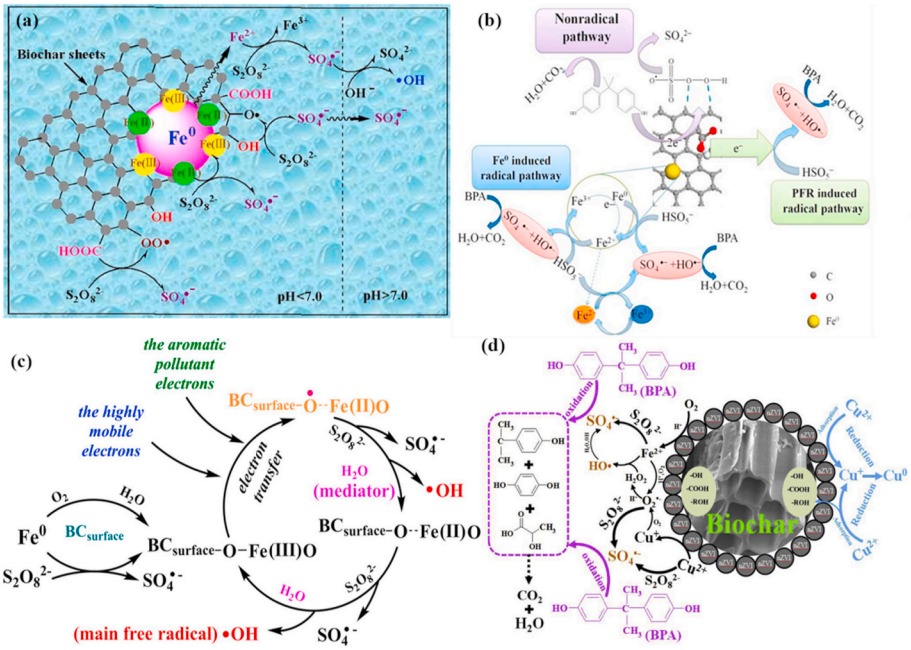

Fig. 2. (a) Proposed mechanism of TCE degradation. Adapted with permission from Ref. (Yan et al., 2015). Copyright 2014 Elsevier. (b) Proposed mechanism of PMS activation by Fe-BC-700. Adapted with permission from Ref. (Jiang et al., 2019), Copyright 2018 Elsevier. (c) Proposed mechanism of the radical pathway in the nZVI/BC_5-PS system. Adapted with permission from Ref. (Luo et al., 2019), Copyright 2018 Elsevier. (d) Possible reaction mechanism for the synergistic reduction of Cu^{2+} and oxidation of BPA by the BC-nZVI/PS system. Adapted with permission from Ref. (Liu et al., 2018), Copyright 2018 Elsevier.

In a related work, Luo et al. (2019) studied the synergistic heterogeneous degradation of aromatic pollutants in alkaline solutions in textile dyeing wastewater by nZVI/BC/PS system. The mechanism was proposed in Fig. 2c. The $BC_{surface}$-OFeO species were confirmed owing to the oxidation-reduction reaction of nZVI with the surface functional groups of BC and PS (Eq. (33) and Eq. (34)), and they produced abundant PFRs (Eq. (35)) which highly enhanced the catalytic activity in an alkaline condition. Aromatic pollutants were absorbed in the nZVI/BC_5 through π-π, π-π-metal ($BC_{surface}$-OFeO) and reacted with $SO_4^{\bullet-}$ and •OH produced by the reaction between $BC_{surface}$-OFeO species and PS or H_2O. Some other pollutant was dislodged through chemisorption. Synergistic effect that combined chemisorption and degradation improved the efficiency of removing aromatic pollutants.

$$BC_{sur.}\text{-}O + 1/2O_2 + Fe^0 \rightarrow BC_{sur.}\text{-}O\text{-}Fe(II)O \quad (33)$$

$$BC_{sur.}\ldots Fe(OH)_2 + S_2O_8^{2-} \rightarrow BC_{sur.}\text{-}O\text{-}Fe(III)O + H_2O + SO_4^{2-} + SO_4^{\bullet-} \quad (34)$$

$$BC_{sur.} - O - Fe(\ddagger)O \xrightarrow{electron} BC_{sur.} - O'Fe(\dagger)O \quad (PFRs) \quad (35)$$

Except for organic pollution, heavy metals pollution is also an urgent environmental problem, and heavy metal and organic compound pollution often exists in the environment that needs to be solved. For example, Chen et al. synthesized a magnetic biochar derived from persulfate-ZVI treated sludge together with one-pot pyrolysis (Chen et al., 2018b). What's exciting is that Liu et al. (2018) first reported the feasibility of BC-nZVI/PS system for the remediation of coexistence of heavy metal and organic compound in aquatic environment. The BC/nZVI/PS system achieved the simultaneous removal of Cu^{2+} and BPA, and 96% of Cu^{2+} and 98% of BPA were removed within 60 min under the condition of 5 mg/L Cu^{2+}, while 80.6% of BPA was degraded without Cu^{2+}, indicating proper concentration of Cu^{2+} could enhance the efficiency of BPA degradation. Two main reasons may be responsible for that: 1) Cu^{2+} accelerated the release of Fe^{2+} via Eq. (36) and Eqs. (37) and (2)) Cu^{2+} can activate PS to generate $SO_4^{\bullet-}$ via Eq. (38). The author proposed a reaction mechanism of the simultaneous removal of Cu^{2+} and BPA by the BC-nZVI/PS system in Fig. 2d. Cu^{2+} and BPA were absorbed on the surface of BC-nZVI, and Cu^{2+} was subsequently removed via Eq. (36) and Eq. (37), while BPA was removed mainly by $SO_4^{\bullet-}$. Besides, $O_2^{\bullet-}$ also taken part in the removal of BPA via Eqs. (39)–(42). Interestingly, Fenton reaction take part in this system because H_2O_2 was generated through the reaction between Fe^{2+} and dissolved oxygen (Eqs. (43)–(45)).

$$Fe^0 + Cu^{2+} \rightarrow Fe^{2+} + Cu^0 \quad (36)$$

$$Fe^0 + 2Cu^{2+} + 2H_2O \rightarrow Fe^{2+} + Cu_2O + H^+ \quad (37)$$

$$2Cu^{2+} + S_2O_8^{2-} \rightarrow SO_4^{\bullet-} + SO_4^{2-} + Cu^{3+} \quad (38)$$

$$S_2O_8^{2-} + 2H_2O/OH^- \rightarrow HO_2^- + 2SO_4^{2-} + 3H^+ \quad (39)$$

$$HO_2^- + S_2O_8^{2-} \rightarrow SO_4^{\bullet-} + O_2^{\bullet-} + SO_4^{2-} + H^+ \quad (40)$$

$$Fe^{2+} + O_2 \rightarrow Fe^{3+} + O_2^{\bullet-} \quad (41)$$

$$O_2^{\bullet-} + S_2O_8^{2-} \rightarrow SO_4^{\bullet-} + SO_4^{2-} + O_2 \quad (42)$$

$$Fe^{2+} + O_2^{\bullet-} + 2H^+ \rightarrow Fe^{3+} + H_2O_2 \quad (43)$$

$$2O_2^{\bullet-} + 2H^+ \rightarrow O_2 + H_2O_2 \quad (44)$$

$$Fe^{2+} + H_2O_2 \rightarrow Fe^{3+} + \bullet OH + OH^- \quad (45)$$

Fe-based catalysts had attracted much attention because of their high natural abundance, low cost, non-toxic, easy synthesis, excellent physicochemical, magnetic properties and environmental friendliness (Ruan et al., 2021). They were widely considered to be one of the best catalysts for activating chemical oxidants to degrade organic pollutants in wastewater (Liu et al., 2022a, 2022b). Furthermore, Fe-based solid catalysts had been extensively used to catalyze chemical oxidants to remove organic matter from wastewater (Wang and Bai, 2017), and Fe-based biochar had attracted extensive attention and more research was put into it. The doping of Fe species changed the surface characteristics of biochar and increased the number of catalytic sites. During the degradation of pollutants, firstly, ROSs played an important role. Fe species including Fe oxide and nZVI were the sources of ferrous ions, and the generated Fe^{2+} activated PS/PMS to produce $SO_4^{\bullet-}$, and then $SO_4^{\bullet-}$ reacted with H_2O/OH^- to produce •OH. In addition, in the process of AOPs, the generation of $O_2^{\bullet-}$ also improved the removal efficiency of pollutants. In addition to the free radical pathway, a non-free radical pathway also existed in the reaction system. For example, the production of $^1O_2$ was also beneficial to the removal of pollutants. Besides, the reduction of Fe^{3+} was attributed to PS/PMS and ROSs. In such a system, the organic contaminant in the wastewater was degraded into small

molecular substances, and finally into CO_2 and H_2O. Unfortunately, the disadvantages of low pH requirements and heavy iron sludge production limited the application of Fe-based AOPs.

3. Cu species modified BC for persulfate catalysis

Cu-modified biochar catalysts have attracted attention because the redox properties of copper are similar to those of iron. For instance, BC-CuO composite material was synthesized by a simple method, and acted as an efficient PMS activator to treat high salt wastewater (Li et al., 2020e). It was found that a Methylene Blue removal efficiency of 99.68% was obtained in BC-CuO/PMS system, which was much higher than single PMS, BC/PMS, and CuO/PMS system. The experimental results showed that •OH, $SO_4^{\bullet-}$, $O_2^{\bullet-}$ and $^1O_2$ were produced during BC-CuO activating PMS. Results also revealed that $^1O_2$ was the main active oxygen in BC/CuO/PMS process. The formation of $^1O_2$ was accelerated by both the oxygen containing functional groups on the surface of biochar and the hydroxylation on the surface of CuO. The possible mechanism of BC-CuO activating PMS to degrade pollutants was proposed, including two pathways. The first was a non-free radical pathway to produce $^1O_2$. On the one hand, the functional groups in biochar such as C–OH and COOH could directly activate PMS to produce $^1O_2$ via Eq. (46) and Eq. (47). On the other hand, semiquinone radicals (BC-semiquinone$^{\bullet-}$) could transfer electron to molecular oxygen to produce $O_2^{\bullet-}$ and quinone groups (BC-quinone) (Fang et al., 2015). As a result, the surface of BC-CuO was hydroxylated and forming Cu^{2+}-OH^- active center in aqueous phase, which can then react with HSO_5^- to form •OH and finally decomposed into $^1O_2$ (Xu et al., 2016). Secondly, the self-decomposition of PMS can also produce $^1O_2$ slowly (Yang et al., 2018). Besides, Cu^{2+} could react with HSO_5^- to form $SO_5^{\bullet-}$ and produced $SO_4^{\bullet-}$ and oxygen, which could promote the production of $^1O_2$ and accelerate the degradation of pollutants (Xu et al., 2016).

$$2BCsurface{-}OOH + 2HSO_5^- \rightarrow 2BCsurface{-}OO^{\bullet-} + 2SO_4^{2-} + {}^1O_2 \quad (46)$$

$$2BCsurface{-}OH + 2HSO_5^- \rightarrow 2BCsurface{-}O^{\bullet-} + 2SO_4^{2-} + {}^1O_2 + 4H^+ (47)$$

Similarly, copper oxide modified rice straw biochar composite (Cu-RSBC) was synthesized by crystal growth method and used to activate PS to degrade phenacetin (PNT) (Li et al., 2020a). Scanning electron microscopy (SEM) and Energy dispersive X-ray spectroscopy spectra of Cu-RSBC showed that the main elements of C, Cu and O were uniformly distributed in the RSBC-CuO catalyst, rather than the random mixture of CuO and RSBC. RSBC-CuO catalyst had a larger specific surface area, which was beneficial to provide more active sites. Compared with RSBC, the catalytic effect of CuO-RSBC was greatly improved. The removal rates of PNT and total organic carbon (TOC) increased from 94.1% to 52%–100% and 64.5% respectively. EPR studies showed that four reactive oxygen species including $SO_4^{\bullet-}$, •OH, $O_2^{\bullet-}$ and $^1O_2$ were participated in the decomposition of PNT. The reactions between $SO_4^{\bullet-}$ and OH^- or H_2O might produce •OH, and $O_2^{\bullet-}$ was produced through Eq. (39) and Eq. (40) similarly, and $^1O_2$ was generated according to Eqs. (48)–(50). The quenching test further proved that O_2 and $O_2^{\bullet-}$ played a key role in the removal of PNT. The catalytic degradation mechanism in the RSBC-CuO/PDS/PNT system was proposed in Fig. 3. It was proposed that the surface oxygen-containing groups bonded with Cu(II) could promote the activation of PS to form $SO_4^{\bullet-}$, as shown in Eq. (51) and Eq. (52). The surface hydroxyl groups bonded to CuO further accelerated the production of $SO_4^{\bullet-}$ through the rapid electron transfer between RSBC-CuO and PS.

$$O_2^{\bullet-} + H_2O \rightarrow \bullet OOH + OH^- \quad (48)$$

$$O_2^{\bullet-} + \bullet OOH \rightarrow {}^1O_2 + OOH^- \quad (49)$$

$$\bullet OOH + \bullet OOH \rightarrow {}^1O_2 + H_2O_2 \quad (50)$$

$$RSBC\text{-}CuO_{sf}\text{-}OOH + S_2O_8^{2-} \rightarrow SO_4^{\bullet-} + RSBC\text{-}CuO_{sf}\text{-}OO^{\bullet-} + HSO_4^- \quad (51)$$

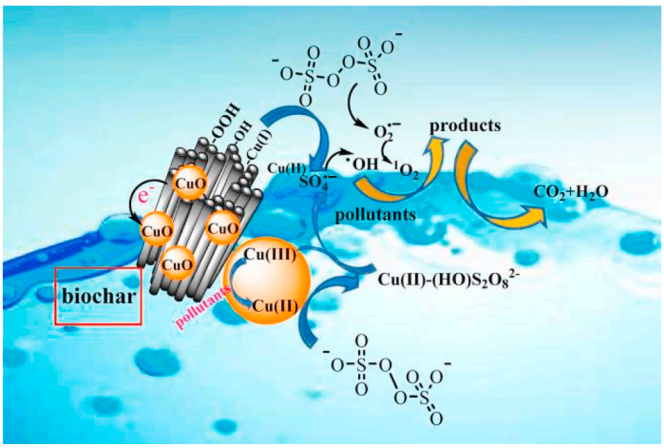

Fig. 3. Schematic illustration of catalytic degradation mechanism in the RSBC-CuO/PDS/PNT system. Adapted with permission from Ref. (Li et al., 2020a), Copyright 2020 Elsevier.

$$RSBC\text{-}CuO_{sf}\text{-}OH + S_2O_8^{2-} \rightarrow SO_4^{\bullet-} + RSBC\text{-}CuO_{sf}\text{-}O^{\bullet-} + HSO_4^- \quad (52)$$

In 2020, Chen et al. (2020) established a simple Cu/BC/PS system to remove TC. Compared with Cu/PS and BC/PS systems, Cu^{2+} effectively increased the surface positive charge of biochar and enhanced the adsorption of TC in Cu/BC/PS system. Cu/BC700/PS system (biochar obtained at 700 °C) could effectively remove TC in a wide pH range and high chemical oxygen demand (COD) concentration. According to radical quenching experiments, the possible charge-transfer mechanism for the degradation of TC in the Cu/BC700/PS system could be shown through the following equations, Eqs. (53)–(57). In this catalytic system, the reduced Cu(I) on biochar was a catalytic center in the degradation process and the $SO_4^{\bullet-}$ and •OH were the dominant radicals.

$$Cu(II) + BC_{surface}\text{-}OOH \rightarrow Cu(I) + BC_{surface}\text{-}OO\bullet + H^+ \quad (53)$$

$$Cu(I) + S_2O_8^{2-} \rightarrow SO_4^{\bullet-} + Cu(II) + SO_4^{2-} \quad (54)$$

$$BC_{surface}\text{-}OO\bullet + S_2O_8^{2-} + H^+ \rightarrow 2SO_4^{\bullet-} + BC_{surface}\text{-}OOH \quad (55)$$

$$SO_4^{\bullet-} + H_2O \rightarrow \bullet OH + SO_4^{2-} + H^+ \quad (56)$$

$$TC\text{-}BC_{surface} \rightarrow BC_{surface} + \text{Degradation products} \quad (57)$$

In a recent work, Zhong et al. (2020) synthesized an N–Cu/biochar with an urchin-like Cu supported on the carbon material of the sheet-like structure. The urchin-like Cu provided a lot of active sites. As shown in Fig. 4, when Cu was heated and evaporated for a long time, the material had a pore size of 10–50 nm, which provided a large number of activation sites for catalytic reaction and functional groups. By comparing the catalytic effects of N/biochar and N–Cu/biochar, it was speculated that Cu may be the main active substance of the system. In addition, nitrogen doping could improve the activity of the catalyst due to the improvement in the electron transfer ability. The results of quenching experiment and electron paramagnetic resonance confirmed that the degradation of TC by •OH was more important than that by $SO_4^{\bullet-}$. In this system, the existence of $^1O_2$ was also observed, indicating the existence of a non-free radical pathway, as shown in Fig. 4. It could be concluded that the main reason for TC degradation was the electron transfer between TC and PS on the surface of the catalyst.

Cu had the advantages of low toxicity, wide valid pH range, relatively low cost, and easy access so Cu-based AOPs had attracted extensive attention (Wang et al., 2022). The mechanism of Cu-based biochar in activating PS/PMS to remove pollutants in wastewater was similar to that of Fe, including $SO_4^{\bullet-}$, •OH, $O_2^{\bullet-}$ and other ROSs, and the production of $^1O_2$, as well as the surface oxygen-containing groups. However, it was

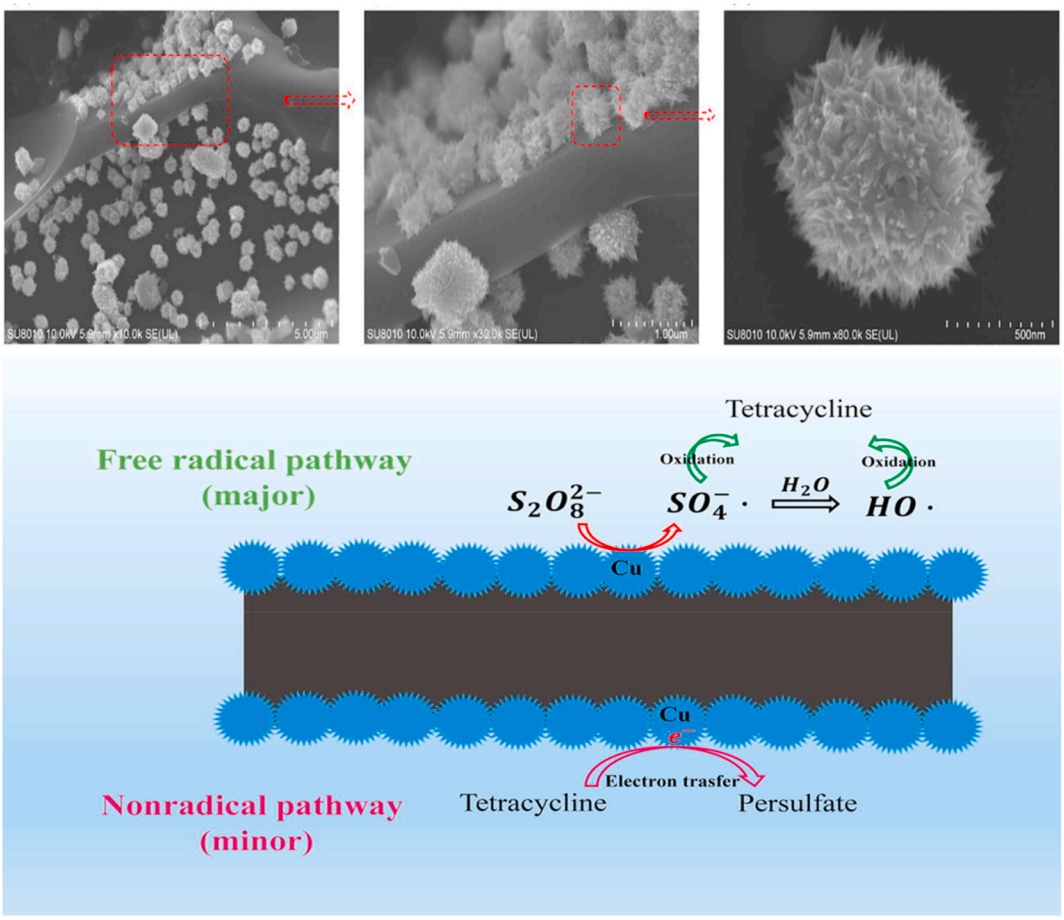

Fig. 4. The surface topography of N–Cu/biochar (a, b, c) and schematic illustration of catalytic degradation mechanism. Adapted with permission from Ref. (Zhong et al., 2020), Copyright 2019 Elsevier.

deserved attention that if the concentration of copper ions exceeded a limit, it will exert adverse effects on the environment and human health. In addition, the recovery of Cu-based biochar was more difficult than magnetic biochar, which limited the application of Cu-based AOPs.

4. Co species modified BC for persulfate catalysis

Apart from Fe, Cu species modified biochar, Co modified biochar has also attracted significant attention for PS catalysis in recent years. For instance, in 2019, Xu et al. (2020) synthesized a biochar-supported Co_3O_4 composite for catalyzing PMS to remove chloramphenicols (CAP). They observed that Co_3O_4 particles were well dispersed on biochar, and the CAP degradation efficiency has been greatly improved. Almost all CAP was removed in the Co_3O_4-BC/PMA system. The author proposed the possible mechanism of PMS activation by Co_3O_4-BC: 1) firstly, BC-Co^{2+} reacts with HSO_5^- to produce $SO_4^{\bullet-}$ and BC-Co^{3+}, 2) the generated BC-Co^{3+} could be reduced to BC-Co^{2+} by HSO_5^-, 3) and meanwhile $SO_4^{\bullet-}$ can react with H_2O and OH^- to generate •OH. During the reaction, $SO_4^{\bullet-}$ played a dominant role, and the redox cycle of Co^{3+}/Co^{2+} was enhanced due to the improved electron transfer between the Co species and HSO_5^- by BC. In another study, Co_3O_4 loaded rice straw derived biochar (BC–Co_3O_4) was used to act as PMS activator for antibiotics degradation (ofloxacin, OFX) (Chen et al., 2018a). Similarly, both $SO_4^{\bullet-}$ and •OH contributed to the OFX degradation. Over 90% of OFX was removed within 10 min in the system. The author summarized two reasons for the improvement of degradation efficiency: 1) more active sites were produced owing to the loading of Co_3O_4 on the large surface area, 2) amounts of Co–OH groups were generated because of the increased O_V and O_A components.

In addition to Co_3O_4, other Co species, such as CoO, Co^0 and Co_9S_8, can be also used to activate PMS/PS. Van-Truc et al. (2019) obtained biochar from spent coffee ground and synthesized Co-impregnated spent coffee ground (Co-SCG) for catalyzing PMS to degrade TC as shown in Fig. 5a. Result indicated that CoO nanoparticles (NPs) were uniformly distributed on biochar and enhanced TC degradation efficiency remarkably: nearly all TC was removed within 25 min in Co-SCG/PMS system. In this system, PMS reacted with Co-SCG to generate $SO_4^{\bullet-}$, which acted as the dominant radical during degradation of the pollutants, and •OH was produced during catalysis process simultaneously. In another study, Luo et al. (2020b) carbonized Co-impregnated goat manure waste and successfully prepared surface-loaded cobalt/biochar (Co-GMC-900) for the first time. The Co^{2+} bound to the lignocellulose in the raw goat manure through chelation (Bo et al., 2019; Luo et al., 2020a), and then the samples were burned in a tube furnace at different temperatures (600, 700, 800, 900 °C) for 2 h. As shown in Fig. 5b, Co^0 NPs were successfully introduced on the surface of biochar. The catalyst exhibited excellent performance in the process of CIP degradation: 96.5% of CIP was removed within 30 min over Co-GMC-900/PMS. The CIP degradation could be attributed to the synergistic effect of free radicals process ($SO_4^{\bullet-}$, •OH and $O_2^{\bullet-}$) and non-free radicals process ($^1O_2$ and charge transfer), as shown in Fig. 5c. Not only $SO_4^{\bullet-}$ and •OH were released via the reaction of PMS and Co^{2+} (Hong et al., 2020), but also $O_2^{\bullet-}$ was produced due to the reaction between Co^{3+} and generated H_2O_2 (Eqs. (58)–(63)). Continuously, the generated radicals achieved efficient degradation of CIP. Apart from the redox cycle of Co^{3+}/Co^{2+}, Co^0/Co^{2+} redox conjugate appeared in the reaction, Co^0 can also react with PMS to generate $SO_4^{\bullet-}$ and •OH directly (Sun et al., 2016), and thus accelerate the conversion of Co^{3+} to Co^{2+} (Eqs. (64)–(66)). Additionally, non-free

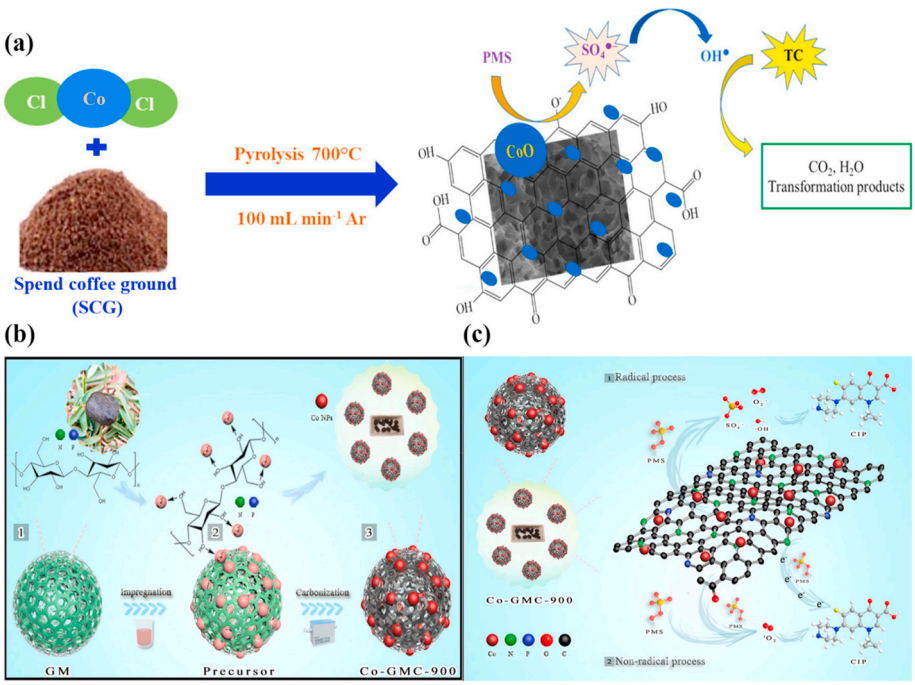

Fig. 5. (a) Schematic illustration for preparing Co-GMC-900 as a catalyst for activating PMS to degrade TC. Adapted with permission from Ref. (Van-Truc et al., 2019), Copyright 2019 Elsevier. (b) The preparation process of Co-GMCs. Adapted with permission from Ref. (Luo et al., 2020b), Copyright 2020 Elsevier. (c) PMS activation mechanism by Co-GMC-900 for CIP degradation. Adapted with permission from Ref. (Luo et al., 2020b), Copyright 2020 Elsevier.

radical processes happened in the system. Owing to the graphitized structure of Co-GMC, electron could transfer from surface to PMS. And $^1O_2$ could be generated by C═O components and decomposition of PMS (Eq. (67)) (Liu et al., 2019a).

$$Co^{2+} + HSO_5^- \rightarrow SO_4^{2-} + Co^{3+} + \bullet OH \quad (58)$$

$$Co^{2+} + HSO_5^- \rightarrow SO_4^{\bullet-} + Co^{3+} + OH^- \quad (59)$$

$$Co^{3+} + HSO_5^- \rightarrow Co^{2+} + SO_5^{\bullet-} + H^+ \quad (60)$$

$$HSO_5^- + H_2O \rightarrow H_2O_2 + HSO_4^- \quad (61)$$

$$Co^{3+} + H_2O_2 \rightarrow Co^{2+} + \bullet HO_2 + H^+ \quad (62)$$

$$\bullet HO_2 \rightarrow O_2^{\bullet-} + H^+ \quad (63)$$

$$Co^0 + HSO_5^- \rightarrow 2\bullet OH + Co^{2+} + 2SO_4^{2-} \quad (64)$$

$$Co^0 + HSO_5^- \rightarrow 2SO_4^{\bullet-} + Co^{2+} + 2OH^- \quad (65)$$

$$Co^0 + 2Co^{3+} \rightarrow 2Co^{2+} \quad (66)$$

$$HSO_5^- + SO_5^{2-} \rightarrow SO_4^{2-} + HSO_4^- + {}^1O_2 \quad (67)$$

Cobalt sulfide (Co_9S_8) also had high catalytic activity for PMS. In 2020, Wang et al. (Wang and Wang, 2020) synthesized CoO/-Co_9S_8@N-S-BC, in which nano Co_9S_8 and CoO were encapsulated by N and S co-doped sludge-derived biochar, by a facile pyrolysis method. Desired cobalt chloride hexahydrate and sublimed sulfur were mixed and stirred, and then biochar was added. Thereafter, the obtained solid was heated by a two-step pyrolysis process under N_2 condition. CoO/-Co_9S_8@N-S-BC/PMS could completely remove 0.08 mM sulfamethoxazole (SMX) within 10 min because of the large number of active sites on the surface of this catalyst, which could significantly improve the efficiency of PMS activation. It was suggested that $SO_4^{\bullet-}$ and •OH were responsible for the degradation of SMX, and all of carbon defects, pyridinic N, quaternary N, the carbon atoms next pyridinic N, C═O groups, -C-S-C and Co(II) were participated in the catalytic profess to produce these radicals, which therefore largely enhanced the degradation efficiency. Interestingly, in addition to the reduction of Co^{3+} by PMS, S^{2-} played a vital role in the reduction of Co^{3+}. Firstly, S^{2-} could directly reduce Co^{3+} to Co^{2+} through Eq. (68). The generated S_2^{2-} would be oxidized to SO_3^{2-} by PMS. SO_3^{2-} could not only reduce Co^{3+} and promote the conversion of Co^{3+} to Co^{2+} (Eq. (69)), but also react with $SO_5^{\bullet-}$ to generate $SO_4^{\bullet-}$ and promote the production of free radical (Eq. (70)). Meanwhile, $SO_3^{\bullet-}$ could be converted into $SO_5^{\bullet-}$ in the presence of oxygen according to Eq. (71). In another study, Yang et al. (2019a) prepared Co-impregnated biochar (CoIB) for PMS catalysis to remove acetaminophen (ACE) by a similar method. Specifically, CO_2 was used instead of N_2 as the reaction medium for pyrolysis of Co/lignin, and the results showed that CoIB had higher catalytic activity. The results show that Co species in the compound were Co_9S_8 NPs and Co NPs. Nearly 90% of ACE was removed by CoIB–CO_2/PMS within 30 min, while only 60% was removed in CoIB–N_2/PMS system. It was proposed that the degradation of ACE was attributed to the combined action of $SO_4^{\bullet-}$ and •OH produced by PMS activated by CoIB.

$$2S^{2-} + 2Co^{3+} \rightarrow 2Co^{2+} + S_2^{2-} \quad (68)$$

$$Co^{3+} + SO_3^{2-} \rightarrow Co^{2+} + SO_3^{\bullet-} \quad (69)$$

$$SO_3^{2-} + SO_5^{\bullet-} \rightarrow SO_4^{\bullet-} + SO_4^{2-} \quad (70)$$

$$SO_3^{\bullet-} + O_2 \rightarrow SO_5^{\bullet-} \quad (71)$$

Co was also an excellent catalyst for activating oxidants (Han et al.), especially Co^{2+} had a high activation effect on PMS. Therefore, most studies were committed to Co-based biochar activating PMS to remove pollutants in wastewater. Similarly, Co-based biochar activated PMS to produce $SO_4^{\bullet-}$ and other ROSs, which played a major role in the removal of organic pollutants. However, as Co was heavy metal, it may have adverse effects on human health. Moreover, the source of Co was not as wide as that of Fe and Cu, and the price was relatively expensive, which limited the application of Co-based biochar.

5. Application of bi-metals-modified biochar in catalytic persulfate removal of contaminants

5.1. Fe–Mn/BC

It is well known that some metal complex catalysts can show higher activity than the corresponding single metal oxides in the activation of PS (Qin et al., 2020). Especially the bimetallic catalysts composed of iron, copper, manganese and cerium, which have attracted extensive attention due to their coupling effect and high valence state. Many studies have shown that bimetallic catalysts have good catalytic performance for refractory organic pollutants, among which iron-based metal complex was the most widely used (Cheng et al., 2019).

In 2019, Fu et al. (2019a) prepared hierarchical porous biochar materials by carbonization of corn stems, leaves and cores (CS/CL/CC) at high temperature, and synthesized $MnFe_2O_4$/biochar composites (MS/ML/MC) by solvothermal method. Experiments results showed that CS had a smooth surface and a large lamellar structure and the fish scale structure of MS resulted in many pores on the surface, and $MnFe_2O_4$ nanoclusters were loaded on the porous layered structure of MS. Otherwise, the degree of graphitization was very important for the activation of PMS, and graphitization was conducive to electron transfer. The catalytic mechanisms which involved three ways were proposed (Fig. 6a): 1) with the participating and coupling of Fe(III)/Fe(II), Mn (III)/Mn(II) and O_2, $O_2^{\bullet-}$, $SO_4^{\bullet-}$ and •OH were produced by one-electron reduction of PMS, 2) through the graphitization structure of $MnFe_2O_4$/MS, electrons were transferred from organic compounds to PMS, which promoted the self-decomposition of PMS and produced a large amount of $^1O_2$ (Sun et al., 2017), 3) the electron could transfer from organic compounds to PMS directly mediated by graphitization structures. Because of the different reduction potentials of $HSO_5^-/SO_5^{\bullet-}$ and Mn(III)/Mn(II), the redox cycle of Mn(III)/Mn(II) was completed through Eq. (72) and Eq. (73), while Fe(III) was reduced by $O_2^{\bullet-}$. It was noteworthy that the reduction of Mn(III) by Fe(II) was thermodynamically favorable and promoted the reduction of Mn(III). More recently, Zhou et al. (2020) prepared a magnetic biochar containing Fe_3O_4 and nano α-MnO_2 (MBM). SEM images showed that α-MnO_2 in the composite was one-dimensional nanorod structure, and the surface of biochar was uniformly covered by Fe_3O_4, which prevented the direct contact between manganese ions and biochar. However, X-ray diffractometer (XRD) analysis showed that the existence of Fe_3O_4 may induce α-MnO_2 crystallization, which was conducive to the loading of α-MnO_2 on MBM. Different from previous studies on manganese, radical quenching experiments and EPR spectra showed that the active substances produced by MBM activating PS were mainly $^1O_2$ (Fig. 6b). It was also suggested that the adsorption of 4-chlorophenol by biochar may shorten the migration path of active substances to pollutant molecules, thus improving the removal rate. In another work, Huang et al. (2020b) also believe that the adsorption of contaminants plays an important role in the degradation of TC by the manganese doped magnetic biochar (MMBC)/PS system. They suggested the adsorption mechanism of TC on MMBC may be the result of hydrogen bonding, π-π electron donor-acceptor interaction and oxygen-containing functional group interaction. In this work, X-ray photoelectron spectroscopy (XPS) results showed that the contents of iron and manganese in different valence states changed during the catalysis, which indicated that there was an electron transfer process on the metal surface. The XPS results also showed that the useful oxygen-containing functional groups on the surface of biochar were C–OH and –COOH, which would be oxidized in the process of providing electrons to PS (Rong et al., 2019; Tang et al., 2018). More interestingly, the authors proposed that the defect structure of carbon material could also activate PS to produce free radicals. The defect structure of nano carbon material interface would reduce the chemical bond energy of O–O bond in PS molecule, leading the structure tended to be unstable (Yao et al., 2019). The oxygen group with high redox potential and edge defects would then promote the electron transfer of the catalyst, and generate more free radicals (Fig. 6c) (Qin et al., 2019).

$$Mn(II) + HSO_5^- \rightarrow Mn(III) + SO_4^{\bullet-} + OH^- \quad (72)$$

$$Mn(III) + HSO_5^- \rightarrow Mn(II) + SO_5^{\bullet-} + OH^- \quad (73)$$

Recently, Hao et al. (2020) used SDBC to prepare Fe–Mn biochar (FM-SDBC) bimetallic composites. The degradation rate of Orange G by FM-SDBC/PS reached 75.23%, which was better than those of Fe-SDBC/PS and Mn-SDBC/PS. The quenching experiment proved that the $SO_4^{\bullet-}$ and •OH were produced in the catalytic process, and the synergistic mechanism of Fe and Mn was also proposed. Fe and Mn would be converted into valence state under the oxidation of PS, forming a cycle (Eqs. (74)–(78)). Moreover, the existence of Fe–Mn bond could accelerate the decomposition of PS and produced free radicals to degrade Orange G (Eq. (79) and Eq. (80)).

$$Fe(II) + S_2O_8^{2-} \rightarrow Fe(III) + SO_4^{\bullet-} + SO_4^{2-} \quad (74)$$

$$Mn(II) + S_2O_8^{2-} \rightarrow Mn(III) + SO_4^{\bullet-} + SO_4^{2-} \quad (75)$$

$$Mn(III) + S_2O_8^{2-} \rightarrow Mn(IV) + SO_4^{\bullet-} + SO_4^{2-} \quad (76)$$

$$Fe(III) + S_2O_8^{2-} \rightarrow Fe(II) + S_2O_8^{\bullet-} \quad (77)$$

$$Mn(IV) + S_2O_8^{2-} \rightarrow Mn(III) + S_2O_8^{\bullet-} \quad (78)$$

$$Mn(III) + Fe(II) \rightarrow Fe(III) + Mn(II) \quad (79)$$

$$Mn(III) + Fe(III) \rightarrow Fe(II) + Mn(IV) \quad (80)$$

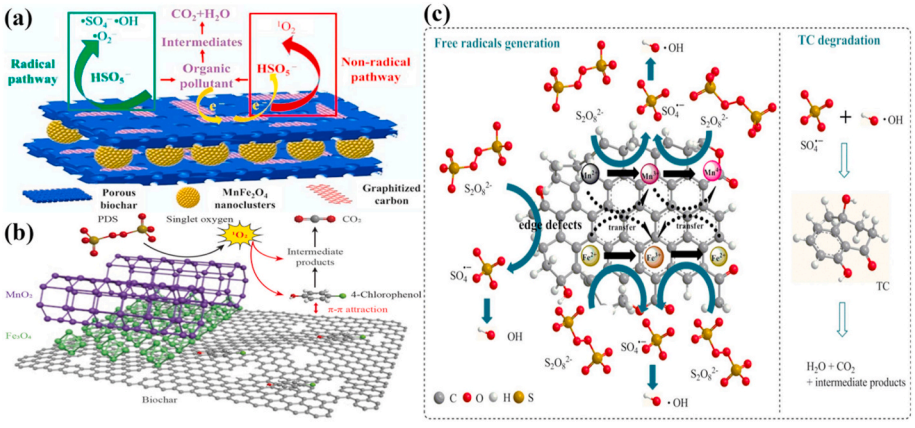

Fig. 6. (a) Mechanism of PMS activation on $MnFe_2O_4$/MS for organic oxidation. Adapted with permission from Ref. (Fu et al., 2019a), Copyright 2018 Elsevier. (b) Proposed catalytic mechanism of PDS activation on MBMS for 4-chlorophenol degradation. Adapted with permission from Ref. (Zhou et al., 2020), Copyright 2020 Elsevier. (c) Main catalytic mechanism of PS activation on MMBC for TC degradation. Adapted with permission from Ref. (Huang et al., 2020b), Copyright 2019 Elsevier.

5.2. Other bi-metals/BC

Apart from Mn, Co also is a good partner of Fe. In 2020, Li et al. (2020d) synthesized a new type of magnetic biochar ($CoFe_2O_4$/HPC) for the catalytic degradation of BPA. The composite had a strong magnetic, multi-stage porous and graphitized structure. The synergistic effect of graphitized structure and $CoFe_2O_4$ were emphasized, and the free radical pathway dominated by sulfate and non-free radical pathway dominated by singlet oxygen were revealed, as well as the secondary role of electron transfer pathway played by graphitized structure. It was suggested despite that the redox potential (1.81 V) of Co(III)/Co(II) was larger than that of $HSO_5^-/SO_5^{\bullet-}$ (1.10 V), Co(II) can be oxidized by HSO_5^- to $SO_4^{\bullet-}$, and the produced Co(III) could be reduced by HSO_5^-, resulting to the efficient regeneration of Co(II). On the other hand, Fe (0.77 V) could be reduced to Fe (II) by $O_2/O_2^{\bullet-}$ (−0.33 V) with low redox potential (Huang et al., 2017b). In addition, Fe(II) could activate HSO_5^- to form $SO_4^{\bullet-}$. Besides, since the redox potential of Co(III)/Co(II) was higher than that of Fe(III)/Fe(II), Fe(II) could reduce Co(III) and further boost the regeneration of Co(II) (Hu and Long, 2016; Zhu et al., 2017b). The formation of $^1O_2$ that also plays an important role in this catalytic system could be divided into three ways: 1) Co(III) oxidized the PMS molecule adsorbed on the surface of $CoFe_2O_4$, and then $SO_5^{\bullet-}$ could react with itself or water to produce $^1O_2$, 2) activated carbon decomposed PMS into $^1O_2$, and 3) the oxidation reaction of PMS molecules adsorbed on the graphitized surface around $CoFe_2O_4$ nanoparticles, and then formed $^1O_2$.

In addition to Fe, Cu, Co and Mn, some biochar modified by other composite metals also have high catalytic efficiency for PS. In 2019, Huang et al. (2019) prepared biochar composite catalyst by calcining Mg–Fe layered double hydroxides (LDHs) produced in the process of Mg–Fe coagulation treatment of piggery wastewater at different temperatures. Biochar was produced in situ in the coagulation process of piggery wastewater. It could introduce a lot of organic matter, bacteria and carbonate to intercalate LDHs. Sludge was calcined under argon atmosphere at different temperatures (such as CS-700), and its catalytic activity for degradation of Tylosin and Rhodamine B (RHB) was investigated. A new possible degradation mechanism was proposed: the chain reaction of free radicals produced different kinds of free radical ions, such as •OH and HO_2^- and so on. All the free radical ions, peroxides and superoxide were the main reasons for the degradation of Tylosin. In the gradient temperature experiment, CS-700 was the best biochar composite catalyst for the complete decolorization of RHB. The main function of biochar was to convert HSO_5^- and oxygen into $SO_4^{\bullet-}$ and $O_2^{\bullet-}$ by using the electrons generated from the redox reaction of iron compounds. However, it's worth noting that after 700 °C oxygen limited pyrolysis, the LDHs structure of CS-700 might be destroyed, and the optimization role of transition metals needed to be further explored.

More recently, Dong et al. (2020) synthesized Fe–Ce/WCSB composite by modified wet chemical method. The composite was used to activate PS to degrade phthalate esters (PAEs) in marine sediments. According to the XRD patterns, it was speculated that there were aromatic rings with enhanced π polarity on the surface of WCSB, which would allow the formation of strong π-electron donor acceptor (π-EDA) interaction with aromatic compounds (Ghaffar et al., 2015). In addition, Ce^{4+} was replaced by Fe^{3+} to form active lattice oxygen, which could form active hydroxyl when bimetallic Fe–Ce was exposed to aqueous solution (Akhtar et al., 2015). Similarly, the degradation of PAE was mainly attributed to $SO_4^{\bullet-}$ and •OH, which were produced by activating PS with Ce^{3+} and Fe^{2+}. Furthermore, $SO_4^{\bullet-}$ reacted with H_2O or OH^- to form •OH. In addition, $O_2^{\bullet-}$ was also produced by Eqs. (81)–(83). After that, Zhu et al. (2020) synthesized biochar supported nano zero valent iron/nickel bimetallic composites (BC@nZVI/Ni) by liquid-phase reduction method to degrade norfloxacin (NOR) in water. SEM images showed that the addition of nickel improves the dispersion of nZVI particles, and nZVI/Ni particles were uniformly dispersed on BC surface. The results of batch experiments in different reaction systems (PS, BC, BC/PS, nZV/Ni, nZVI/Ni/PS and nZVI/Ni/PS) showed that the degradation of NOR was mainly because BC@nZVI/Ni/polystyrene system produces free radicals for oxidation, or PS direct oxidation and nZVI/Ni reduction, rather than adsorption. The proposed degradation mechanism was shown in Fig. 7. It further confirmed that $SO_4^{\bullet-}$ was the main free radical in acidic and neutral conditions, while •OH played an important role in alkaline conditions. In addition, BC played an important role in the BC@nZVI/Ni/PS system, because the C–OOH and C–OH groups on BC surface could also activate PS to form $SO_4^{\bullet-}$.

$$S_2O_8^{2-} + H_2O \rightarrow HO_2^- + 2SO_4^{2-} + 3H^+ \quad (81)$$

$$HO_2^- + 2SO_4^{2-} \rightarrow SO_4^{\bullet-} + SO_4^{2-} + H^+ + O_2^{\bullet-} \quad (82)$$

$$S_2O_8^{2-} + 2H_2O \rightarrow SO_4^{\bullet-} + 3SO_4^{2-} + 4H^+ + O_2^{\bullet-} \quad (83)$$

Bi-metallic catalysts exhibited higher activity than the corresponding single metals or their oxides in activating PS/PMS, which may be due to the interaction between bimetallic (Fu et al., 2022). Fe and Mn bimetallic biochar attracted more interest because of its low toxicity, magnetism, high efficiency, good stability, and rich value state. The mechanism of bi-metallic catalyst-activated PS/PMS to remove pollutants was similar to that of single metal, including the free radical pathway and the non-free radical pathway. In particular, due to the different redox potentials, one metal ion can be reduced by another metal ion, such as Mn^{3+} could be reduced by Fe^{2+}. The synergistic mechanism of bi-metal-modified biochar-based AOPs and detailed degradation process deserved further study and explanation.

6. Conclusion and prospects

Biochar, which has excellent physical properties and economic practicality, has attracted extensive attention of researchers. Compared with some other AOP processes, the AOP using the biochar has its unique characteristics, as shown in Table 2. In this study, the recent studies of transition metal-modified biochar catalysts in PS activation for pollutant removal are reviewed. The concept of transition metals or their oxides-modified biochar for catalytic applications offers several potential advantages over single biochar or transition metals. These composite materials not only combine the respective beneficial characteristics of biochar and transition metals (or their oxides) but also often present synergistic effects between the components. The porous structure of biochar enables the uniform distribution of transition metals (or their oxides) and improves their stability in aqueous solution, while the latter can not only improve the catalytic activity of biochar but also increase the concentration of PERs in biochar. Also, in some cases, the loading of magnetic metal oxides can make the catalyst easy to recycle. In these catalytic systems, PMS/PS can be activated by both the biochar and the

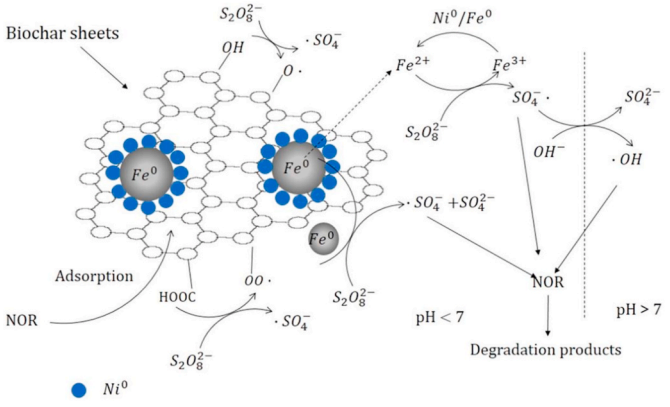

Fig. 7. Proposed mechanism of NOR degradation using BC@nZVI/N/PS system. Adapted with permission from Ref. (Zhu et al., 2020), Copyright 2020 Elsevier.

Table 1
Main applications of metal-loaded biochar catalysts in Fenton-like processes for the remove of pollutants involved in this paper.

Catalysts	Reaction systems	Pollutants	Reaction conditions	Performance	Mechanism	Ref.
nFe_3O_4/BC	nFe_3O_4/BC + PS	1, 4-dioxane	the composite mass ratio of 1:1 between nFe_3O_4 and biochar pyrolyzed at 400 °C, initial neutral pH	98% of 1, 4-dioxane was removed.	$SO_4^{\bullet-}$ and •OH were responsible for the remove of 1, 4-dioxane.	Ouyang et al. (2017)
γ-Fe_2O_3@BC	γ-Fe2O3@BC + PS	BPA	$[BPA]_0$ = 20 mg/L, T = 25 °C,	A complete remove of BPA was achieved. Catalytic activity decreased after 4 recycles.	•OH was the dominant active species.	Rong et al. (2019)
Fe-N-BC	Fe-N-BC + PS	AO7	$[AO7]_0$ = 20 mg/L, pH_0 = 3.0	Almost all AO7 was degraded.	$O_2^{\bullet-}$, •OH, $SO_4^{\bullet-}$ and $^1O_2$ participated in the degradation of AO7	Li et al. (2020b)
OBC-Fe_3O_4	OBC-Fe_3O_4 + PS	TC	$[TC]_0$ = 20 mg/L, pH = 3.0	92.3% of TC was removed. Catalytic activity slightly decreased after 3 recycles.	•OH and $SO_4^{\bullet-}$ played dominant role.	Pi et al. (2019)
Fe_3O_4/MC	Fe_3O_4/MC + PMS	HBA	$[HBA]_0$ = 10 mg/L, T = 25 °C	Almost all HBA was removed. Catalytic activity significantly decreased after 3 recycles.	$SO_4^{\bullet-}$ played a vital role.	Fu et al. (2019b)
MS-BC	MS-BC + PDS	TC	$[TC]_0$ = 100 mg/L, pH = 2.17	82.24% of TC degraded. Catalytic activity slightly decreased after 3 recycles.	•OH and $SO_4^{\bullet-}$ participated in the removal of TC.	Yu et al. (2019)

Catalysts	Reaction systems	Pollutants	Reaction conditions	Performance	Mechanism	Ref.
nZVI/BC	nZVI/BC + PS	TCE	$[TCE]_0$ = 0.15 mM, pH = 6.3	The degradation efficiency of TCE was 99.4%.	$SO_4^{\bullet-}$ accounted for TCE degradation.	Yan et al. (2015)
ZVI-SDBC	ZVI-SDBC + PS	AO7	$[AO7]_0$ = 0.06 mM, pH_0 = 5.22	99.0% of AO7 was removed. Catalytic activity slightly decreased after 3 recycles.	$SO_4^{\bullet-}$, •OH and $^1O_2$ contributed to AO7 degradation.	Wang et al. (2020)
BC-nZVI	BC-nZVI + PS	Cu^{2+}/BPA	$[Cu^{2+}]_0$ = 5 mg/L, $[BPA]_0$ = 10 mg/L, pH = 3.0 ± 0.2	The efficiencies of Cu^{2+} and BPA reached 96% and 98%.	$SO_4^{\bullet-}$ and $O_2^{\bullet-}$ were responsible for BPA degradation, and Cu^{2+} was reduced.	Liu et al. (2018)
RSBC-CuO	RSBC-CuO + PDS	PNT	$[PNT]_0$ = 10 mg/L, pH = 4.26, T = 25 °C	PNT was completely decomposed. Catalytic activity declined slightly after 4 cycles.	$^1O_2$ and $O_2^{\bullet-}$ played the crucial role in the PNT removal.	Li et al. (2020a)
Cu/BC700	Cu/BC700 + PS	TC	$[TC]_0$ = 120 mg/L, pH = 4-9	The degradation efficiencies were 55.4%, 62.9%, 72.6% under a pH of 4.0, 7.0, 9.0, respectively. Catalytic activity decreased slightly after 5 cycles.	$SO_4^{\bullet-}$ and •OH contributed to the TC degradation.	Chen et al. (2020)
N–Cu/BC	N–Cu/BC + PS	TC	$[TC]_0$ = 20 mg/L, pH = 7.0	All the TC was removed. Catalytic activity decreased after 2nd and 3rd runs.	•OH played a crucial role for TC degradation.	Zhong et al. (2020)

Catalysts	Reaction systems	Pollutants	Reaction conditions	Performance	Mechanism	Ref.
Co_3O_4-BC	Co_3O_4-BC + PMS	CAP	$[CAP]_0$ = 30 mg/L, pH = 7	CAP was nearly completely removed. Good performance even after 10-cycle runs.	$SO_4^{\bullet-}$ played a dominant role in CAP degradation.	Xu et al. (2020)
Co_3O_4-BC	Co_3O_4-BC + Oxone	OFX	$[OFX]_0$ = 50 μM, pH = 7, T = 25 °C	Over 90% of OFX was removed. Catalytic activity significantly decreased during the second run.	•OH played a major role for OFX degradation.	Chen et al. (2018a)
Co-SCG	Co-SCG + PMS	TC	$[TC]_0$ = 0.2 mM, pH = 7.0	TC was almost completely degraded. No obvious loss of catalytic activity even after 10 cycles.	$SO_4^{\bullet-}$ and •OH contributed to the TC degradation.	Van-Truc et al. (2019)
Co-GMC-900	Co-GMC-900 + PMS	CIP	$[CIP]_0$ = 20 mg/L, pH = 6.3, T = 25 °C	96.5% of CIP was removed. Catalytic activity decreased slightly even after 5 cycles.	$SO_4^{\bullet-}$, •OH, $O_2^{\bullet-}$ and $^1O_2$ contributed to CIP degradation.	Luo et al. (2020b)
CoO/Co_9S_8@N-S-BC	CoO/Co_9S_8@N-S-BC + PMS	SMX	$[SMX]_0$ = 0.08 mM, pH = 3.0, T = 25 °C	SMX was complete removed. Catalytic activity decreased slightly even after 5 cycles.	$SO_4^{\bullet-}$ and •OH contributed to the SMX degradation.	Wang and Wang (2020)
CoIB	CoIB + PMS	ACE	$[ACE]_0$ = 5 mg/L, T = 30 °C	Over 90% of ACE was removed. No obvious loss of catalytic activity after 4 cycles.	$SO_4^{\bullet-}$ and •OH contributed to the ACE degradation.	Yang et al. (2019a)

Catalysts	Reaction systems	Pollutants	Reaction conditions	Performance	Mechanism	Ref.
$MnFe_2O_4$/MS	$MnFe_2O_4$/MS + PMS	Orange II	[orange II]$_0$ = 20 mg/L, pH_0 = 5.8, T = 25 °C	Orange II was completely removed. Catalytic activity significantly decreased during the second and third cycle.	$SO_4^{\bullet-}$, •OH and $^1O_2$ contributed to orange II degradation.	Fu et al. (2019a)
MBM	MBM + PS	4-CP	$[4\text{-CP}]_0$ = 10 mg/L	4-CP was completely removed. Catalytic activity declined after 2nd and 3rd runs.	$^1O_2$ played a vital role for 4-CP degradation.	Zhou et al. (2020)

(*continued on next page*)

Table 1 (*continued*)

Catalysts	Reaction systems	Pollutants	Reaction conditions	Performance	Mechanism	Ref.
MMBC	MMBC + PS	TC	$[TC]_0$ = 20 mg/L, pH = 3, T = 25 °C	93% of TC was removed. Catalytic activity decreased slightly after 4 cycles.	$SO_4^{\bullet-}$ and •OH contributed to the TC degradation.	[120]
$CoFe_2O_4$/HPC	$CoFe_2O_4$/HPC + PMS	BPA	$[BPA]_0$ = 10 mg/L, pH_0 = 7.4, T = 25 °C	All BPA could be removed. Catalytic activity decreased slightly even after 4 cycles.	$SO_4^{\bullet-}$ and $^1O_2$ contributed to the Orange G degradation.	Li et al. (2020d)
Fe–Ce/WCSB	Fe–Ce/WCSB + PS	PAEs	$[sediment]_0$ = 1 g, pH_0 = 6.0, molar ratio of PS to ∑PAEs = 1:1, T = 30 °C	Almost all PAEs were removed.	$SO_4^{\bullet-}$ was responsible for PAEs degradation.	Dong et al. (2020)
BC@nZVI/Ni	BC@nZVI/Ni + PS	NOR	$[NOR]_0$ = 10 mg/L, pH = 3 ± 0.2	80.5% of NOR was removed.	$SO_4^{\bullet-}$ and $^1O_2$ contributed to the NOR degradation.	Zhu et al. (2020)

Table 2
The advantages/disadvantages of AOP using the biochar and comparison with some other materials.

Materials	Advantages	Disadvantages	Ref.
Transition metal-modified biochar	Wide range of raw materials and low cost, High specific surface area and high porosity, Abundant functional groups, Excellent adsorption and catalytic efficiency.	Metal ion leaching, Diffusion of materials during application.	(Qin et al., 2020; Wang et al., 2021)
Transition metal oxide	Strong redox ability, Inexpensive and easy to obtain.	Difficulties in recovery, Secondary pollution to the environment, Sensitive to pH changes.	(Feng et al., 2013; Wu et al., 2021; Wang and Wang, 2018)
MOFs (Metal-organic frameworks)	Large specific surface area, Ultra-high porosity, Diversity of material design.	Weak conductivity, Susceptible to high temperature or strong current, The reaction under UV irradiation reduces the efficiency, Stable deviation.	(Huang et al., 2021b; Huang et al., 2021a; Liu et al., 2021a, 2021b)
LDH (Layered double hydroxide)	Structural stability, Adjustable composition, structure and electronic properties.	Low conductivity, Poor electron and charge transfer capability, Insufficient active edge position.	(Yang et al., 2020; Ge et al., 2022; Xie et al., 2021)
G (Graphene)	Large specific surface area, Excellent conductivity, Well chemical stability.	High cost, Difficult to recycle.	(Nidheesh, 2017; Wang et al., 2019c)
CNTs (carbon nanotubes)	Large specific surface areas, Excellent electrical conductivity characteristics, Low-cost synthesis	Poor separability	(Peng et al., 2021; Wu et al., 2022)

metallic compound, which result in the production of a large number of $SO_4^{\bullet-}$ and •OH, and thus improve the degradation efficiency of pollutants.

In addition to free radical pathway, non-free radical pathway also existed in catalytic system widely. In the non-free radical pathway, both the increase of electron transfer rate and the generation of $^1O_2$ contributed to the degradation. What's more, the structure of materials changed due to the loading of metal, which enhanced the degradation efficiency.

Due to the distinct advantages of transition metals (or their oxides)/biochar composites, these materials will provide a unique opportunity for the development of alternative catalysts for SR-AOPs. However, despite that many progresses have been made, this research field is still at the early stage and more effort should be dedicated before these catalysts can be industrially applied. Future studies can be extended to:

1) Transition metal-modified biochar/PS system has a good removal effect on pollutants, and this technology can be combined with other technologies such as photocatalysis (Wu et al., 2020) and biotechnology (Zhu et al., 2017a) in the actual wastewater treatment process.
2) There are also some problems in the application of these materials, such as the diffusion of materials and metal seepage, and they will be eliminated with the supernatant entrainment. Recent studies reported an interesting system called "Galvanic oxidation process (GOP)", in which catalyst was coated onto graphite electrodes and PMS and target water were separated into two half cells, for the remote activation of PMS by catalyst when they are physically separated. This system might help solve such problems. GOP could overcome many challenges in traditional PMS-based AOPs, such as difficulty in the catalyst recovery, chemical addition to the treated water, unnecessary PMS consumption, and so on. In general, given its advantages over traditional processing technology, it may be a promising development direction for BC-based catalysts (Huang and Zhang, 2019, 2020).
3) Because most of the experiments are limited to the laboratory, there may be deviation in the actual project operation. In order to avoid this situation, large-scale evaluation of biochar catalyst and its economy should be encouraged to obtain more realistic data.
4) The large-scale synthesis of biochar requires higher quality technology and equipment. In addition, it's necessary to compare the different biomass, and use suitable raw materials to synthesize biochar according to the situation of different regions.
5) Excepted for water pollution, soil pollution and air pollution are also makes a serious threat to human safety and natural environment. SR-AOP catalyzed metal-loaded biochar has been widely concerned in water treatment research, but its application in other pollution remediation also deserves attention.
6) Biochar materials may cause damage to the environment in the actual application process, thus it's important to study the environmental risk assessment of it. It can include its transport and transformation in the environment, as well as its potential toxicity.
7) The modified biochar sometimes harms the adsorption of pollutants, further research needs to focus on the mechanism and improve the adsorption efficiency by changing the physical and chemical properties of the adsorbent.

Declaration of competing interest

The authors declare that they have no known competing financial interests or personal relationships that could have appeared to influence

the work reported in this paper.

Acknowledgements

This study was financially supported by the Program for the National Natural Science Foundation of China (51909084, 51909085), and China Postdoctoral Science Foundation Funded Project (2018M642977), the Natural Science Foundation of Hunan Province, China (2020JJ5055, 2020JJ5069), and the Fundamental Research Funds for the Central Universities (531118010247).

References

Akhtar, A., et al., 2015. Electrocatalytic hydrogen production by bulk and nano Fe2O3 and carbon nanotube modified with Fe2O3. J. Electroanal. Chem. 739, 73–83.
Arnold, W., et al., 2017. QSARs for phenols and phenolates: oxidation potential as a predictor of reaction rate constants with photochemically produced oxidants. Abstr. Pap. Am. Chem. Soc. 253.
Arunakumara, K.K.I.U., et al., 2013. Current status of heavy metal contamination in Asia's rice lands. Rev. Environ. Sci. Biotechnol. 12, 355–377.
Bo, S., et al., 2019. Circular utilization of Co(II) adsorbed composites for efficient organic pollutants degradation by transforming into Co/N-doped carbonaceous catalyst. J. Clean. Prod. 236, 117630.
Chen, J., et al., 2020. Removal of tetracycline via the synergistic effect of biochar adsorption and enhanced activation of persulfate. Chem. Eng. J. 382, 122916.
Chen, L., et al., 2018a. Biochar modification significantly promotes the activity of Co3O4 towards heterogeneous activation of peroxymonosulfate. Chem. Eng. J. 354, 856–865.
Chen, Y.-d., et al., 2019. Magnetic biochar catalysts from anaerobic digested sludge: production, application and environment impact. Environ. Int. 126, 302–308.
Chen, Y.-d., et al., 2018b. Lead removal by a magnetic biochar derived from persulfate-ZVI treated sludge together with one-pot pyrolysis. Bioresour. Technol. 247, 463–470.
Cheng, M., et al., 2018a. Metal-organic frameworks for highly efficient heterogeneous Fenton-like catalysis. Coord. Chem. Rev. 368, 80–92.
Cheng, M., et al., 2019. Prussian blue analogue derived magnetic Cu-Fe oxide as a recyclable photo-Fenton catalyst for the efficient removal of sulfamethazine at near neutral pH values. Chem. Eng. J. 362, 865–876.
Cheng, M., et al., 2017. Salicylic acid-methanol modified steel converter slag as heterogeneous Fenton-like catalyst for enhanced degradation of alachlor. Chem. Eng. J. 327, 686–693.
Cheng, M., et al., 2018b. Efficient degradation of sulfamethazine in simulated and real wastewater at slightly basic pH values using Co-SAM-SCS/H2O2 Fenton-like system. Water Res. 138, 7–18.
Cheng, M., et al., 2018c. High adsorption of methylene blue by salicylic acid-methanol modified steel converter slag and evaluation of its mechanism. J. Colloid Interface Sci. 515, 232–239.
Cheng, M., et al., 2016. Hydroxyl radicals based advanced oxidation processes (AOPs) for remediation of soils contaminated with organic compounds: a review. Chem. Eng. J. 284, 582–598.
Deng, J., et al., 2017. Heterogeneous activation of peroxymonosulfate using ordered mesoporous Co3O4 for the degradation of chloramphenicol at neutral pH. Chem. Eng. J. 308, 505–515.
Deng, Y., et al., 2018. Facile fabrication of mediator-free Z-scheme photocatalyst of phosphorous-doped ultrathin graphitic carbon nitride nanosheets and bismuth vanadate composites with enhanced tetracycline degradation under visible light. J. Colloid Interface Sci. 509, 219–234.
Dong, C.-D., et al., 2017. Synthesis of magnetic biochar from bamboo biomass to activate persulfate for the removal of polycyclic aromatic hydrocarbons in marine sediments. Bioresour. Technol. 245, 188–195.
Dong, C.-D., et al., 2018a. Wood-biochar-supported magnetite nanoparticles for remediation of PAH-contaminated estuary sediment. Catalysts 8 (2), 73.
Dong, C.-D., et al., 2020. Degradation of phthalate esters in marine sediments by persulfate over Fe–Ce/biochar composites. Chem. Eng. J. 384, 123301.
Dong, C.-D., et al., 2019. Degradation of 4-nonylphenol in marine sediments by persulfate over magnetically modified biochars. Bioresour. Technol. 281, 143–148.
Dong, C.-D., et al., 2018b. Remediation and cytotoxicity study of polycyclic aromatic hydrocarbon-contaminated marine sediments using synthesized iron oxide-carbon composite. Environ. Sci. Pollut. Res. 25, 5243–5253.
Du, Y., et al., 2020. Efficient removal of acid orange 7 using a porous adsorbent-supported zero-valent iron as a synergistic catalyst in advanced oxidation process. Chemosphere 244, 125522.
Duan, X., et al., 2015. Insights into heterogeneous catalysis of persulfate activation on dimensional-structured nanocarbons. ACS Catal. 5, 4629–4636.
Duan, X., et al., 2018. Metal-free carbocatalysis in advanced oxidation reactions. Accounts Chem. Res. 51, 678–687.
Faheem, et al., 2020. Application of biochar in advanced oxidation processes: supportive, adsorptive, and catalytic role. Environ. Sci. Pollut. Res. 27, 37286–37312.
Fang, G., et al., 2015. Mechanism of hydroxyl radical generation from biochar suspensions: implications to diethyl phthalate degradation. Bioresour. Technol. 176, 210–217.
Feng, Y., et al., 2013. Iron oxide catalyzed fenton-like reaction. Prog. Chem. 25, 1219–1228.
Fu, H., et al., 2019a. Activation of peroxymonosulfate by graphitized hierarchical porous biochar and MnFe2O4 magnetic nanoarchitecture for organic pollutants degradation: structure dependence and mechanism. Chem. Eng. J. 360, 157–170.
Fu, H., et al., 2019b. Fabrication of Fe3O4 and graphitized porous biochar composites for activating peroxymonosulfate to degrade p-hydroxybenzoic acid: insights on the mechanism. Chem. Eng. J. 375, 121980.
Fu, W.H., et al., 2022. When bimetallic oxides and their complexes meet Fenton-like process. J. Hazard Mater. 424.
Ge, L., et al., 2022. Layered double hydroxide based materials applied in persulfate based advanced oxidation processes: property, mechanism, application and perspectives. J. Hazard Mater. 424, 127612.
Ghaffar, A., et al., 2015. Effect of biochar aging on surface characteristics and adsorption behavior of dialkyl phthalates. Environ. Pollut. 206, 502–509.
Giannakis, S., et al., 2021. A review of the recent advances on the treatment of industrial wastewaters by Sulfate Radical-based Advanced Oxidation Processes (SR-AOPs). Chem. Eng. J. 406, 127083.
Han, S., et al., Oxidative degradation of tetracycline using peroxymonosulfate activated by cobalt-doped pomelo peel carbon composite. Environ. Sci. Pollut. Res.
Hao, H., et al., 2020. Insight into the degradation of Orange G by persulfate activated with biochar modified by iron and manganese oxides: synergism between Fe and Mn. J. Water Proc. Eng. 37, 101470.
Hayat, W., et al., 2019. Efficient degradation of imidacloprid in water through iron activated sodium persulfate. Chem. Eng. J. 370, 1169–1180.
Hong, Y., et al., 2020. Heterogeneous activation of peroxymonosulfate by CoMgFe-LDO for degradation of carbamazepine: efficiency, mechanism and degradation pathways. Chem. Eng. J. 391, 123604.
Hu, C., et al., 2018. The combination of Fenton process and Phanerochaete chrysosporium for the removal of bisphenol A in river sediments: mechanism related to extracellular enzyme, organic acid and iron. Chem. Eng. J. 338, 432–439.
Hu, P., Long, M., 2016. Cobalt-catalyzed sulfate radical-based advanced oxidation: a review on heterogeneous catalysts and applications. Appl. Catal. B Environ. 181, 103–117.
Huang, D., et al., 2017a. Combination of Fenton processes and biotreatment for wastewater treatment and soil remediation. Sci. Total Environ. 574, 1599–1610.
Huang, D., et al., 2020a. Optimal preparation of catalytic Metal-organic framework derivatives and their efficient application in advanced oxidation processes. Chem. Eng. J. 421, 127817.
Huang, D., et al., 2021b. Progress and challenges of metal-organic frameworks-based materials for SR-AOPs applications in water treatment. Chemosphere 263, 127672.
Huang, D., et al., 2021a. Optimal preparation of catalytic Metal-organic framework derivatives and their efficient application in advanced oxidation processes. Chem. Eng. J. 421, 127817.
Huang, D., et al., 2020b. Mn doped magnetic biochar as persulfate activator for the degradation of tetracycline. Chem. Eng. J. 391, 123532.
Huang, G.-X., et al., 2017b. Degradation of bisphenol A by peroxymonosulfate catalytically activated with Mn1.8Fe1.2O4 nanospheres: synergism between Mn and Fe. Environ. Sci. Technol. 51, 12611–12618.
Huang, Z., et al., 2019. Coagulation treatment of swine wastewater by the method of in-situ forming layered double hydroxides and sludge recycling for preparation of biochar composite catalyst. Chem. Eng. J. 369, 784–792.
Huang, K.Z., Zhang, H., 2019. Direct electron-transfer-based peroxymonosulfate activation by iron-doped manganese oxide (delta-MnO2) and the development of galvanic oxidation processes (GOPs). Environ. Sci. Technol. 53, 12610–12620.
Huang, K.Z., Zhang, H., 2020. Galvanic oxidation processes (GOPs): an effective direct electron transfer approach for organic contaminant oxidation. Sci. Total Environ. 743, 140828.
Hussain, I., et al., 2017. Insights into the mechanism of persulfate activation with nZVI/BC nanocomposite for the degradation of nonylphenol. Chem. Eng. J. 311, 163–172.
Ji, F., et al., 2011. Performance of CuO/Oxone system: heterogeneous catalytic oxidation of phenol at ambient conditions. Chem. Eng. J. 178, 239–243.
Jiang, S.-F., et al., 2019. High efficient removal of bisphenol A in a peroxymonosulfate/iron functionalized biochar system: mechanistic elucidation and quantification of the contributors. Chem. Eng. J. 359, 572–583.
Khachatryan, L., et al., 2011. Environmentally persistent free radicals (EPFRs). 1. Generation of reactive oxygen species in aqueous solutions. Environ. Sci. Technol. 45, 8559–8566.
Lee, C.-S., et al., 2018. Zerovalent-iron/platinum janus micromotors with spatially separated functionalities for efficient water decontamination. ACS Appl. Nano Mater. 1, 768–776.
Lee, J.E., Park, Y.-K., 2020. Applications of modified biochar-based materials for the removal of environment pollutants: a mini review. Sustainability Basel 12 (15), 6112.
Li, H., et al., 2017. Mechanisms of metal sorption by biochars: biochar characteristics and modifications. Chemosphere 178, 466–478.
Li, W., et al., 2020a. Efficient activation of peroxydisulfate (PDS) by rice straw biochar modified by copper oxide (RSBC-CuO) for the degradation of phenacetin (PNT). Chem. Eng. J. 395, 125094.
Li, X., et al., 2020b. High-efficiency degradation of organic pollutants with Fe, N co-doped biochar catalysts via persulfate activation. J. Hazard Mater. 397, 122764.
Li, X., et al., 2020c. Preparation and application of magnetic biochar in water treatment: a critical review. Sci. Total Environ. 711, 134847.
Li, Y., et al., 2020d. Novel magnetic biochar as an activator for peroxymonosulfate to degrade bisphenol A: emphasizing the synergistic effect between graphitized structure and CoFe2O4. Chem. Eng. J. 387, 124094.

Li, Z., et al., 2020e. Biochar supported CuO composites used as an efficient peroxymonosulfate activator for highly saline organic wastewater treatment. Sci. Total Environ. 721, 137764.
Ling, S.K., et al., 2010. Oxidative degradation of dyes in water using Co2+/H2O2 and Co2+/peroxymonosulfate. J. Hazard Mater. 178, 385–389.
Liu, C.-M., et al., 2018. Simultaneous removal of Cu2+ and bisphenol A by a novel biochar-supported zero valent iron from aqueous solution: synthesis, reactivity and mechanism. Environ. Pollut. 239, 698–705.
Liu, C., et al., 2019a. From rice straw to magnetically recoverable nitrogen doped biochar: efficient activation of peroxymonosulfate for the degradation of metolachlor. Appl. Catal. B Environ. 254, 312–320.
Liu, H., et al., 2022a. Modified UiO-66 as photocatalysts for boosting the carbon-neutral energy cycle and solving environmental remediation issues. Coord. Chem. Rev. 458, 214428.
Liu, J., et al., 2022b. Preparation, characterization, and applications of Fe-based catalysts in advanced oxidation processes for organics removal: a review. Environ. Pollut. 293, 118565.
Liu, Y., et al., 2021a. The application of Zeolitic imidazolate frameworks (ZIFs) and their derivatives based materials for photocatalytic hydrogen evolution and pollutants treatment. Chem. Eng. J. 417, 127914.
Liu, Y., et al., 2021b. Polyoxometalate@Metal-Organic framework composites as effective photocatalysts. ACS Catal. 11, 13374–13396.
Liu, Y., et al., 2019b. Heterogeneous Fenton-like catalyst for treatment of rhamnolipid-solubilized hexadecane wastewater. Chemosphere 236, 124387.
Liu, Y., et al., 2020. Metal sulfide/MOF-based composites as visible-light-driven photocatalysts for enhanced hydrogen production from Water splitting. Coord. Chem. Rev. 409, 213220.
Liu, Y., et al., 2017. Effect of rhamnolipid solubilization on hexadecane bioavailability: enhancement or reduction? J. Hazard Mater. 322, 394–401.
Lopes, R.P., Astruc, D., 2021. Biochar as a support for nanocatalysts and other reagents: recent advances and applications. Coord. Chem. Rev. 426, 213585.
Luo, H., et al., 2019. New insights into the formation and transformation of active species in nZVI/BC activated persulfate in alkaline solutions. Chem. Eng. J. 359, 1215–1223.
Luo, J., et al., 2020a. Designing ordered composites with confined Co-N/C layers for efficient pollutant degradation: structure-dependent performance and PMS activation mechanism. Microporous Mesoporous Mater. 293, 109810.
Luo, J., et al., 2020b. Transforming goat manure into surface-loaded cobalt/biochar as PMS activator for highly efficient ciprofloxacin degradation. Chem. Eng. J. 395, 125063.
Maria-Hormigos, R., et al., 2018. Carbon nanotubes- ferrite- manganese dioxide micromotors for advanced oxidation processes in water treatment. Environ. Sci. Nano. 5, 2993–3003.
Ngoc Han, T., et al., 2018. Occurrence and fate of emerging contaminants in municipal wastewater treatment plants from different geographical regions-a review. Water Res. 133, 182–207.
Nidheesh, P.V., 2017. Graphene-based materials supported advanced oxidation processes for water and wastewater treatment: a review. Environ. Sci. Pollut. Res. 24, 27047–27069.
Oh, W.-D., et al., 2016. Generation of sulfate radical through heterogeneous catalysis for organic contaminants removal: current development, challenges and prospects. Appl. Catal. B Environ. 194, 169–201.
Ouyang, D., et al., 2017. Degradation of 1,4-dioxane by biochar supported nano magnetite particles activating persulfate. Chemosphere 184, 609–617.
Pan, X., et al., 2021. Preparation of biochar and biochar composites and their application in a Fenton-like process for wastewater decontamination: a review. Sci. Total Environ. 754, 142104.
Pang, H., et al., 2019. Adsorptive and reductive removal of U(VI) by Dictyophora indusiate-derived biochar supported sulfide NZVI from wastewater. Chem. Eng. J. 366, 368–377.
Peng, J., et al., 2021. The carbon nanotubes-based materials and their applications for organic pollutant removal: a critical review. Chin. Chem. Lett. 32, 1626–1636.
Petrie, B., et al., 2015. A review on emerging contaminants in wastewaters and the environment: current knowledge, understudied areas and recommendations for future monitoring. Water Res. 72, 3–27.
Pi, Z., et al., 2019. Persulfate activation by oxidation biochar supported magnetite particles for tetracycline removal: performance and degradation pathway. J. Clean. Prod. 235, 1103–1115.
Premarathna, K.S.D., et al., 2019. Biochar-based engineered composites for sorptive decontamination of water: a review. Chem. Eng. J. 372, 536–550.
Qin, F., et al., 2020. Degradation of sulfamethazine by biochar-supported bimetallic oxide/persulfate system in natural water: performance and reaction mechanism. J. Hazard Mater. 398, 122816.
Qin, J., et al., 2019. Cow manure-derived biochar: its catalytic properties and influential factors. J. Hazard Mater. 371, 381–388.
Ren, W., et al., 2021. Origins of electron-transfer regime in persulfate-based nonradical oxidation processes. Environ. Sci. Technol. 56 (1), 78–97.
Rong, X., et al., 2019. The magnetic biochar derived from banana peels as a persulfate activator for organic contaminants degradation. Chem. Eng. J. 372, 294–303.
Ruan, X., et al., 2019. Formation, characteristics, and applications of environmentally persistent free radicals in biochars: a review. Bioresour. Technol. 281, 457–468.
Ruan, Y., et al., 2021. Review on the synthesis and activity of iron-based catalyst in catalytic oxidation of refractory organic pollutants in wastewater. J. Clean. Prod. 321, 128924.
Sanchez-Polo, M., et al., 2013. Comparative study of the photodegradation of bisphenol A by HO center dot, SO4 center dot- and CO3 center dot-/HCO3 center dot radicals in aqueous phase. Sci. Total Environ. 463, 423–431.
Sun, H., et al., 2017. Activation of peroxymonosulfate by nitrogen-functionalized sludge carbon for efficient degradation of organic pollutants in water. Bioresour. Technol. 241, 244–251.
Sun, H., et al., 2016. One-pot hydrothermal synthesis of octahedral CoFe/CoFe2O4 submicron composite as heterogeneous catalysts with enhanced peroxymonosulfate activity. J. Mater. Chem. A. 4, 9455–9465.
Sun, Y., et al., 2019. Multifunctional iron-biochar composites for the removal of potentially toxic elements, inherent cations, and hetero-chloride from hydraulic fracturing wastewater. Environ. Int. 124, 521–532.
Takdastan, A., et al., 2018. Efficient activation of peroxymonosulfate by using ferroferric oxide supported on carbon/UV/US system: a new approach into catalytic degradation of bisphenol A. Chem. Eng. J. 331, 729–743.
Tan, C., et al., 2014. Radical induced degradation of acetaminophen with Fe3O4 magnetic nanoparticles as heterogeneous activator of peroxymonosulfate. J. Hazard Mater. 276, 452–460.
Tang, L., et al., 2018. Enhanced activation process of persulfate by mesoporous carbon for degradation of aqueous organic pollutants: electron transfer mechanism. Appl. Catal. B Environ. 231, 1–10.
Ushani, U., et al., 2020. Sulfate radicals-based advanced oxidation technology in various environmental remediation: a state-of-the–art review. Chem. Eng. J. 402, 126232.
Van-Truc, N., et al., 2019. Cobalt-impregnated biochar (Co-SCG) for heterogeneous activation of peroxymonosulfate for removal of tetracycline in water. Bioresour. Technol. 292, 121954.
Wang, C., et al., 2021. A review on persulfates activation by functional biochar for organic contaminants removal: synthesis, characterizations, radical determination, and mechanism. J. Environ. Chem. Eng. 9, 106267.
Wang, J., Bai, Z., 2017. Fe-based catalysts for heterogeneous catalytic ozonation of emerging contaminants in water and wastewater. Chem. Eng. J. 312, 79–98.
Wang, J., Wang, S., 2018. Activation of persulfate (PS) and peroxymonosulfate (PMS) and application for the degradation of emerging contaminants. Chem. Eng. J. 334, 1502–1517.
Wang, J., et al., 2020. One-step preparation of ZVI-sludge derived biochar without external source of iron and its application on persulfate activation. Sci. Total Environ. 714, 136728.
Wang, L., et al., 2022. A review on advanced oxidation processes homogeneously initiated by copper(II). Chem. Eng. J. 427, 131721.
Wang, R.-Z., et al., 2019a. Recent advances in biochar-based catalysts: properties, applications and mechanisms for pollution remediation. Chem. Eng. J. 371, 380–403.
Wang, S., Wang, J., 2020. Peroxymonosulfate activation by Co9S8@ S and N co-doped biochar for sulfamethoxazole degradation. Chem. Eng. J. 385, 123933.
Wang, S., et al., 2019b. Biochar-supported nZVI (nZVI/BC) for contaminant removal from soil and water: a critical review. J. Hazard Mater. 373, 820–834.
Wang, X., et al., 2019c. A review of graphene-based nanomaterials for removal of antibiotics from aqueous environments. Environ. Pollut. 253, 100–110.
Wu, L., et al., 2022. Carbon nanotube-based materials for persulfate activation to degrade organic contaminants: properties, mechanisms and modification insights. J. Hazard Mater. 431, 128536.
Wu, S., et al., 2021. Sulfite-based advanced oxidation and reduction processes for water treatment. Chem. Eng. J. 414, 128872.
Wu, T., et al., 2020. Application of QD-MOF composites for photocatalysis: energy production and environmental remediation. Coord. Chem. Rev. 403, 213097.
Xiao, S., et al., 2020. Iron-mediated activation of persulfate and peroxymonosulfate in both homogeneous and heterogeneous ways: a review. Chem. Eng. J. 384, 123265.
Xiao, X., et al., 2018. Insight into multiple and multilevel structures of biochars and their potential environmental applications: a critical review. Environ. Sci. Technol. 52, 5027–5047.
Xie, Z.-H., et al., 2021. Synthesis, application and catalytic performance of layered double hydroxide based catalysts in advanced oxidation processes for wastewater decontamination: a review. Chem. Eng. J. 414, 128713.
Xu, H., et al., 2020. Heterogeneous activation of peroxymonosulfate by a biochar-supported Co3O4 composite for efficient degradation of chloramphenicols. Environ. Pollut. 257, 113610.
Xu, Y., et al., 2016. The mechanism of degradation of bisphenol A using the magnetically separable CuFe2O4/peroxymonosulfate heterogeneous oxidation process. J. Hazard Mater. 309, 87–96.
Yan, J., et al., 2015. Biochar supported nanoscale zerovalent iron composite used as persulfate activator for removing trichloroethylene. Bioresour. Technol. 175, 269–274.
Yang, F., et al., 2018. Peroxymonosulfate/base process in saline wastewater treatment: the fight between alkalinity and chloride ions. Chemosphere 199, 84–88.
Yang, M.-T., et al., 2019a. Cobalt-impregnated biochar produced from CO2-mediated pyrolysis of Co/lignin as an enhanced catalyst for activating peroxymonosulfate to degrade acetaminophen. Chemosphere 226, 924–933.
Yang, X., et al., 2019b. Surface functional groups of carbon-based adsorbents and their roles in the removal of heavy metals from aqueous solutions: a critical review. Chem. Eng. J. 366, 608–621.
Yang, Z.-z., et al., 2020. Design and engineering of layered double hydroxide based catalysts for water depollution by advanced oxidation processes: a review. J. Mater. Chem. A. 8, 4141–4173.
Yao, C., et al., 2019. Insights into the mechanism of non-radical activation of persulfate via activated carbon for the degradation of p-chloroaniline. Chem. Eng. J. 362, 262–268.
Yu, J., et al., 2019. Magnetic nitrogen-doped sludge-derived biochar catalysts for persulfate activation: internal electron transfer mechanism. Chem. Eng. J. 364, 146–159.

Yuan, Y., et al., 2017. Applications of biochar in redox-mediated reactions. Bioresour. Technol. 246, 271–281.
Zhang, G., et al., 2020. Megamerger of MOFs and g-C(3)N(4)for energy and environment applications: upgrading the framework stability and performance. J. Mater. Chem. A. 8, 17883–17906.
Zhang, T., et al., 2013. Production of sulfate radical from peroxymonosulfate induced by a magnetically separable CuFe2O4 spinel in water: efficiency, stability, and mechanism. Environ. Sci. Technol. 47, 2784–2791.
Zhong, Q., et al., 2020. Oxidative degradation of tetracycline using persulfate activated by N and Cu codoped biochar. Chem. Eng. J. 380, 122608.
Zhou, D., et al., 2018. Transition metal catalyzed sulfite auto-oxidation systems for oxidative decontamination in waters: a state-of-the-art minireview. Chem. Eng. J. 346, 726–738.
Zhou, H., et al., 2020. Magnetic biochar supported α-MnO2 nanorod for adsorption enhanced degradation of 4-chlorophenol via activation of peroxydisulfate. Sci. Total Environ. 724, 138278.
Zhou, Z., et al., 2019. Persulfate-based advanced oxidation processes (AOPs) for organic-contaminated soil remediation: a review. Chem. Eng. J. 372, 836–851.
Zhu, F., et al., 2020. Degradation mechanism of norfloxacin in water using persulfate activated by BC@nZVI/Ni. Chem. Eng. J. 389, 124276.
Zhu, X., et al., 2017a. Effects and mechanisms of biochar-microbe interactions in soil improvement and pollution remediation: a review. Environ. Pollut. 227, 98–115.
Zhu, Z., et al., 2017b. Adsorption-intensified degradation of organic pollutants over bifunctional alpha-Fe@carbon nanofibres. Environ. Sci. Nano. 4, 302–306.
Zou, J., et al., 2013. Rapid acceleration of ferrous iron/peroxymonosulfate oxidation of organic pollutants by promoting Fe(III)/Fe(II) cycle with hydroxylamine. Environ. Sci. Technol. 47, 11685–11691.